

1 **Fluxes of Atmospheric Greenhouse-Gases in Maryland (FLAGG-MD):**  
2 **Emissions of Carbon Dioxide in the Baltimore, MD-Washington, D.C. area**

3 **D. Y. Ahn<sup>1</sup>, J. R. Hansford<sup>2</sup>, S. T. Howe<sup>3,1</sup>, X. R. Ren<sup>3,4,5</sup>, R. J. Salawitch<sup>1,3,4</sup>, N. Zeng<sup>3,4</sup>, M.**  
4 **D. Cohen<sup>5</sup>, B. Stunder<sup>5</sup>, O. E. Salmon<sup>6\*</sup>, P. B. Shepson<sup>6,7</sup>, K. R. Gurney<sup>8</sup>, T. Oda<sup>9,10</sup>, I.**  
5 **Lopez-Coto<sup>11</sup>, J. Whetstone<sup>12</sup>, R. R. Dickerson<sup>3</sup>**

6 <sup>1</sup>Department of Chemistry and Biochemistry, University of Maryland College Park, Maryland,  
7 USA, <sup>2</sup>Department of Computer Science, University of Maryland College Park, MD, USA,  
8 <sup>3</sup>Department of Atmospheric and Oceanic Science, University of Maryland College Park, MD,  
9 USA, <sup>4</sup>Earth System Science Interdisciplinary Center, University of Maryland College Park, MD,  
10 USA, <sup>5</sup>National Oceanic and Atmospheric Administration Air Resource Laboratory, College  
11 Park, MD, USA, <sup>6</sup>Department of Chemistry, Purdue University, West Lafayette, IN, USA,  
12 <sup>7</sup>School of Marine and Atmospheric Sciences, Stony Brook University, Stony Brook, NY, USA,  
13 <sup>8</sup>School of Informatics, Computing, and Cyber Systems, Northern Arizona University, Flagstaff,  
14 AZ, USA, <sup>9</sup>Global Modeling and Assimilation Office, NASA Goddard Space Flight Center,  
15 Greenbelt, MD, USA, <sup>10</sup>Goddard Earth Sciences Research and Technology, Universities Space  
16 Research Association, Columbia, MD, USA, <sup>11</sup>Engineering Laboratory, National Institute of  
17 Standards and Technology, Gaithersburg, MD, USA, <sup>12</sup>Special Programs Office, National  
18 Institute of Standards and Technology, Gaithersburg, MD, USA, <sup>1</sup>Now at Areté, Arlington, VA,  
19 USA, \*Now at Lake Michigan Air Directors Consortium, Madison, WI, USA

20 Corresponding author: Doyeon Ahn ([aahndo@umd.edu](mailto:aahndo@umd.edu))

21 **Key Points:**

- 22 • 1.9±0.3 MtC of fossil fuel CO<sub>2</sub> was emitted in Baltimore-Washington during February  
23 2015 based on data collected during 7 aircraft flights
- 24 • 4 bottom-up inventories indicate 2.2±0.3 MtC of fossil fuel CO<sub>2</sub> was emitted, in good  
25 agreement with our top-down estimate
- 26 • The uncertainty from a single flight segment was ±38% (1σ); data from 7 flights yielded  
27 a precision of 16% at the 95% confidence level

28 **Abstract**

29 To study emissions of CO<sub>2</sub> in the Baltimore, MD-Washington, D.C. (Balt-Wash) area, an aircraft  
30 campaign was conducted in February 2015, as part of the FLAGG-MD (Fluxes of Atmospheric  
31 Greenhouse-Gases in Maryland) project. During the campaign, elevated mole fractions of CO<sub>2</sub>  
32 were observed downwind of the urban center and local power plants. Upwind flight data and  
33 HYSPLIT (Hybrid Single Particle Lagrangian Integrated Trajectory) model analyses help  
34 account for the impact of emissions outside the Balt-Wash area. The accuracy, precision, and  
35 sensitivity of CO<sub>2</sub> emissions estimates based on the mass balance approach were assessed for  
36 both power plants and cities. Our estimates of CO<sub>2</sub> emissions from two local power plants agree  
37 well with their CEMS (Continuous Emissions Monitoring Systems) records. For the 16 power  
38 plant plumes captured by the aircraft, the mean percentage difference of CO<sub>2</sub> emissions was  
39 -0.3 %. For the Balt-Wash area as a whole, the 1σ CO<sub>2</sub> emission rate uncertainty for any  
40 individual aircraft-based mass balance approach experiment was ±38 %. Treating the mass

41 balance experiments, which were repeated seven times within nine days, as individual  
42 quantifications of the Balt-Wash CO<sub>2</sub> emissions, the estimation uncertainty was  $\pm 16\%$  (standard  
43 error of the mean at 95% CL). Our aircraft-based estimate was compared to various bottom-up  
44 fossil fuel CO<sub>2</sub> (FFCO<sub>2</sub>) emission inventories. Based on the FLAGG-MD aircraft observations,  
45 we estimate  $1.9 \pm 0.3$  MtC of FFCO<sub>2</sub> from the Balt-Wash area during the month of February 2015.  
46 The mean estimate of FFCO<sub>2</sub> from the four bottom-up models was  $2.2 \pm 0.3$  MtC.

## 47 **1 Introduction**

48 A major increase in the atmospheric abundance of CO<sub>2</sub> since the industrial revolution—with  
49 significant positive perturbation to the radiative forcing of climate—has resulted in a rise of  
50 global mean surface temperature over the past century (Stocker et al., 2013). A large number of  
51 studies that clarified the detrimental impact of global warming and resulting climate change on  
52 Earth’s ecosystem have spurred individual nations to mitigate greenhouse gas (GHG) emissions  
53 under the Paris Climate Agreement (Salawitch et al., 2017). Along with the efforts by most of  
54 the world’s nations, the role of cities in GHG mitigation has become even more important given  
55 the recent U.S. federal decision to pull back from the Paris Climate Agreement (UN, 2017).  
56 Currently, the state of Maryland is on track for reducing consumption-basis GHG emissions by  
57 25% in 2020 and 40% in 2030 relative to emissions in 2006 (MDE, 2015). Washington, D.C. has  
58 set a plan to reduce consumption-basis GHG emissions by 50% in 2032 and by 100% in 2050  
59 relative to 2006 emissions (DOEE, 2018).

60 With increasing GHG mitigation efforts, scientific research to improve the quantification and  
61 attribution of carbon sources in urban areas has become more important (Duren & Miller, 2012;  
62 Hutyra et al., 2014; Patarasuk et al., 2016). According to UN-Habitat (2011), more than 70% of  
63 global CO<sub>2</sub> emissions related to energy usage comes from urban areas. Also, measuring CO<sub>2</sub> in  
64 urban areas is more tractable than measuring CO<sub>2</sub> in countries, because the CO<sub>2</sub> signal from  
65 cities is intense and localized (Gratani & Varone, 2005; Idso et al., 2001). Various measurement  
66 techniques, data analyses, and modeling methods have been collectively used to study CO<sub>2</sub>  
67 emission in urban areas. Among many U.S. cities, the Indianapolis area was chosen as one of the  
68 first testbed sites to develop and evaluate a framework to study urban GHG emissions, given its  
69 relatively simple topography and isolation from other large cities (Davis et al., 2017; Whetstone,  
70 2018). The Indianapolis Flux Experiment (INFLUX, [https://www.nist.gov/topics/greenhouse-  
71 gas-measurements/indianapolis-flux-experiment](https://www.nist.gov/topics/greenhouse-gas-measurements/indianapolis-flux-experiment)) has successfully developed and improved the  
72 mass-balance method and the inversion framework, called “Top-down” approaches, as well as  
73 inventory data-based emission models such as Hestia, a “Bottom-up” approach (Gurney et al.,  
74 2017; Lauvaux et al., 2016; Turnbull et al., 2015, 2018; Whetstone, 2018). Along with INFLUX,  
75 several projects with similar aims have been conducted in other cities. The Megacities Carbon  
76 Project was designed to quantify carbon emissions in some of the world’s largest cities, including  
77 Los Angeles, Paris, and San Paulo (Bréon et al., 2015; Feng et al., 2016; Newman et al., 2016).  
78 Urban GHG emissions from the Boston area (Sargent et al., 2018) and Salt Lake City (McKain et  
79 al., 2012; Strong et al., 2011) have also been extensively investigated.

80 The Fluxes of Atmospheric Greenhouse-Gases in Maryland (FLAGG-MD) project is part of the  
81 National Institute for Standards and Technology (NIST) U.S. Northeast Corridor testbed which,  
82 in its first phase, is focused on the Baltimore, Maryland (MD)-Washington, D.C. (Balt-Wash)  
83 area (Lopez-Coto et al., 2017; Mueller et al., 2018; [https://www.nist.gov/topics/northeast-  
84 corridor-urban-test-bed](https://www.nist.gov/topics/northeast-corridor-urban-test-bed)). Taking a lead from the successful deployment of INFLUX, the

85 FLAGG-MD project aims to understand and quantify emissions of CO<sub>2</sub>, CH<sub>4</sub>, and CO in the  
86 Balt-Wash area. While FLAGG-MD is similar in many ways to INFLUX, the geography of the  
87 Balt-Wash area engenders the following complications. The Balt-Wash area is part of the U.S.  
88 Northeast Corridor, which includes other major cities such as Boston, New York City, and  
89 Philadelphia. Also, the Balt-Wash area is located southeast of the Appalachian Mountains and  
90 northwest of the Chesapeake Bay, such that mesoscale circulations complicate the atmospheric  
91 transport of urban GHG emissions. Several large power plants upwind of the Balt-Wash area can  
92 episodically increase the spatiotemporal variability of the background mole fractions of CO<sub>2</sub>.  
93 The Balt-Wash urban testbed consists mainly of aircraft campaigns conducted in collaboration  
94 with Purdue University (Lopez-Coto et al., 2020; Ren et al., 2018; Salmon et al., 2017, 2018),  
95 along with several other assets: installations of low cost CO<sub>2</sub> sensors (Martin et al., 2017),  
96 meteorological data assimilation, modeling of tower-based observations (Martin et al., 2019;  
97 Mueller et al., 2018) and incorporation of data from the Orbiting Carbon Observatory 2 (OCO-2).

98 In this study, emissions of CO<sub>2</sub> from the Balt-Wash area are quantified using the FLAGG-MD  
99 aircraft campaign dataset obtained during the month of February 2015. Section 2 describes the  
100 aircraft campaign, the mass balance approach, and various models used in this study. In section  
101 3.1, source apportionment of the plumes of CO<sub>2</sub> observed by the aircraft is presented. In section  
102 3.2, the impact of plume transport from out-of-state power plants on the aircraft observations is  
103 investigated. In section 3.3, the accuracy and precision of the aircraft-based mass balance  
104 estimates are evaluated using the Continuous Emissions Monitoring Systems (CEMS) records of  
105 two local power plants. Section 3.4 discusses the uncertainty from mass balance parameters. In  
106 section 3.5, differences in the CO<sub>2</sub> emission rate among our mass balance estimate, other  
107 previously published bottom-up/downscaling model estimates, and the state of Maryland  
108 emission inventory are investigated.

## 109 **2 Methods**

### 110 **2.1 Instrumentation**

111 The University of Maryland (UMD) Cessna 402B aircraft was equipped with a cavity ring-down  
112 spectroscopic (CRDS) analyzer (Picarro Model G2401-m) that is used to measure the dry air  
113 mole fraction of CO<sub>2</sub>. Measurements of CO<sub>2</sub> were calibrated on the ground as well as during the  
114 flight using an onboard calibration system with two cylinders of standard gases certified by  
115 National Institute of Standards and Technology (NIST). These cylinders contained CO<sub>2</sub> of  
116 369.19 and 445.78  $\mu\text{mol mol}^{-1}$  (parts per million, or ppm). A diaphragm pump was installed to  
117 pull the ambient air from the nose of the Cessna through a rear-facing Perfluoroalkoxy alkanes  
118 (PFA) Teflon tube (O.D=0.95 cm and I.D=0.64 cm), at a total flow rate of 10 L/min. The CRDS  
119 analyzer was connected to the main sample line via a Tee connection, allowing air to be pumped  
120 continuously through the analyzer at a rate of 400 mL/min. We tested the stability of the analyzer  
121 by sampling a tank of breathing air continuously while the aircraft climbed from 50 to 3500 m  
122 altitude – the standard deviations of CO<sub>2</sub> were very small, near the measurement precision limit  
123 of the Picarro instrument. The UMD aircraft was also equipped with instruments to measure SO<sub>2</sub>,  
124 NO<sub>2</sub>, NO, O<sub>3</sub>, aerosols, and meteorological variables. A more detailed description on the  
125 instrumentation can be found in Ren et al. (2018). The Purdue Duchess aircraft was equipped  
126 with a CRDS analyzer (Picarro Model G2301-m) for measurements of CO<sub>2</sub> and a Best Air  
127 Turbulence (BAT) probe for measurements of the three-dimensional wind field. A more detailed

128 description of the instrumentation on the Purdue Duchess aircraft can be found in Salmon et al.  
129 (2018).

130 To examine the sensitivity of our mass-balance emission estimation of CO<sub>2</sub> emissions (described  
131 in section 2.5) to the measurement uncertainties, 1 $\sigma$  uncertainties of the temperature, pressure,  
132 and CO<sub>2</sub> mole fraction measurements were propagated into the mass balance equation. The 1 $\sigma$   
133 absolute uncertainty of temperature measurements from both UMD and Purdue flight  
134 instruments was determined to be 2.0 K, based upon a comparison of temperature measurements  
135 made from the two aircraft during a wingtip-to-wingtip flight segment conducted on 19 February  
136 2015. For the 1 $\sigma$  uncertainty of the pressure measurements for the UMD flights, the reported  
137 instrument uncertainty of 0.25 hPa was used. For the Purdue flights, 1 $\sigma$  uncertainty was  
138 determined to be 1.6 hPa based upon a comparison of measured pressure versus calculated  
139 barometric pressure. For the 1 $\sigma$  uncertainty of the CO<sub>2</sub> measurements, the reported instrument  
140 uncertainty of 0.1 ppm was used for data collected by both the UMD and Purdue instruments.

## 141 **2.2 Aircraft research flight design**

142 For this study, the Balt-Wash area is defined as a rectangularly-shaped region enclosed by the  
143 four coordinates of 38.23°N 76.67°W, 39.46°N 75.86°W, 39.87°N 77.04°W, 38.63°N 77.86°W  
144 (154×111 km<sup>2</sup>, see Figure 1). The defined study area consists of large populated regions, within  
145 and surrounding the cities of Baltimore, MD and Washington, D.C. The total population within  
146 the study area was 8,153,000 in year 2015 based on Gridded Population of the World (GPWv4)  
147 data (CIESIN, 2018). Seven major power plants (all within either the states of Maryland or  
148 Virginia) and a dense road network including major highways such as the Capital Beltway ring  
149 (I-495), the Baltimore Beltway (I-695), and interstate highway I-95 all lie within the study area.  
150 According to the Maryland GHG inventory, total of 18.8 MtC (Million tons Carbon) of Fossil  
151 Fuel CO<sub>2</sub> (FFCO<sub>2</sub>) was emitted from Maryland during year 2014 (MDE, 2016).

152 The UMD aircraft conducted a total of nine research flights (UMD RF1-9) in February 2015.  
153 Figure 1 shows all of these flight tracks and Figure S1 shows individual flight tracks. During  
154 seven research flights (UMD RF1-6 and RF8) northwesterly winds prevailed, while a  
155 northeasterly wind was present on UMD RF9 and a southwesterly wind occurred on UMD RF7.  
156 For all flights, the UMD aircraft departed from the Tipton airport (located between Washington,  
157 D.C. and Baltimore) and first flew a horizontal transect upwind of the study area to sample the  
158 incoming air. For the downwind transects of UMD-RF1-6 and RF8, an imaginary vertical plane  
159 AB was defined at the location where polluted plumes from the major emission sources—power  
160 plants, the I-95 highway, and the Washington, D.C., and Baltimore, MD metropolitan areas—  
161 could be sampled separately under northwesterly wind condition (see Figure 1). The aircraft  
162 made multiple horizontal transects at different altitudes in the plane AB to capture the outgoing  
163 air. Several vertical profiles were taken to measure vertical distribution of trace gases and to  
164 estimate the planetary boundary layer (PBL) height. For UMD-RF9, the sampling at downwind  
165 transects at various altitudes was conducted along the plane BC, since this flight was conducted  
166 under northeasterly winds. Data from UMD-RF7 are not used below because of the complex  
167 wind patterns prevalent in the study area on 24 February 2015.

168 The Purdue aircraft conducted a total of six research flights between 16 February to 11 March  
169 2015 (Salmon et al., 2017, 2018) (Figure 1 and S1). Purdue flight tracks were designed in a  
170 similar manner to the UMD flights, aiming to measure mole fractions of CO<sub>2</sub> upwind and  
171 downwind of the Balt-Wash area. On 19 February 2015 (Purdue-RF3), the Purdue aircraft was

172 coordinated with the UMD aircraft (UMD-RF4) to conduct direct comparisons of in-situ  
 173 measurements of CO<sub>2</sub>, other GHGs, and meteorological variables during a wing-tip to wing-top  
 174 segment that lasted about 40 minutes.

### 175 **2.3 HYSPLIT transport modeling**

176 In this study, the Hybrid Single Particle Lagrangian Integrated Trajectory (HYSPLIT) model was  
 177 used to determine the sources of polluted plumes observed from the aircraft (Draxler et al., 1997;  
 178 Stein et al., 2015). A series of back trajectories starting at the aircraft locations, at one second  
 179 intervals, was computed using the default model configuration setup and NAM12 (North  
 180 American Mesoscale Forecast System, 12 km horizontal resolution) as input meteorology.  
 181 Forward transport modeling of power plant CO<sub>2</sub> plumes was conducted using HYSPLIT particle  
 182 dispersion mode with NAM4 (4 km horizontal resolution). The number of particles released per  
 183 cycle (variable name ‘numpar’) was set to 10<sup>6</sup>. The output mass was divided by air density to  
 184 obtain mole fraction (ichem=6). Horizontal grid spacing was specified as 0.1°, given that the  
 185 objective of the modeling is to understand the inter-state transport of power plant plumes in the  
 186 eastern U.S. Vertical grid spacing was set at 100 m below 2000 m and at 500 m above 2000 m.  
 187 All other configuration parameters were set at default values, as described in Draxler et al.  
 188 (2014). As input emission sources, we used power plants listed in the Environmental Protection  
 189 Agency’s Clean Air Markets Division (EPA CAMD) datasets for Washington, D.C., Maryland,  
 190 Pennsylvania, Virginia, West Virginia, and Ohio. The EPA CAMD emission dataset of facility-  
 191 level hourly CO<sub>2</sub> emissions records was obtained from the Air Markets Program Data (AMPD)  
 192 query system (USEPA AMPD, 2015).

### 193 **2.4 VEGAS modeling and NDVI data**

194 A VEgetation-Global Atmospheric-Soil (VEGAS) model simulation was used to calculate the  
 195 biogenic flux of CO<sub>2</sub> over the Balt-Wash area during February 2015. VEGAS is a dynamic soil  
 196 and vegetation model that simulates the growth of plant functional types based on meteorological  
 197 data (Zeng et al., 2004, 2005). The model was run hourly at 9 km resolution using re-gridded  
 198 NARR (North American Regional Reanalysis) data as meteorological input. The simulation was  
 199 started in the year 1715 to provide a spin-up time for regional carbon pools.

200 In addition to the benefit of estimating the biogenic CO<sub>2</sub> flux for the study domain, gridded  
 201 VEGAS biogenic CO<sub>2</sub> flux output was combined with the Normalized Difference Vegetation  
 202 Index (NDVI) data to investigate the impact of biogenic CO<sub>2</sub> emissions on the background CO<sub>2</sub>  
 203 that is needed for the mass balance calculation (see section 3.5.1). Since the VEGAS model was  
 204 not specifically designed to compute biogenic emissions of CO<sub>2</sub> in regions with complex  
 205 landscapes such as the Balt-Wash study area, we have combined VEGAS output with NDVI data  
 206 acquired within the study region during February 2015. First, gridded VEGAS output of net  
 207 biogenic CO<sub>2</sub> flux was computed for the entire Balt-Wash study area. Next, version v1r12 NDVI  
 208 data (4 km, weekly, <https://www.star.nesdis.noaa.gov/smcd/emb/vci/VH/index.php>) from the  
 209 Visible Infrared Imaging Radiometer Suite (VIIRS) on the Suomi National polar-orbiting  
 210 partnership (Suomi-NPP) was summed within each of the narrow grid boxes (NDVI<sup>GRID BOX</sup>)  
 211 perpendicular to line AB as shown in Figure S2. Then, the horizontal transect of the biogenic  
 212 flux of CO<sub>2</sub> within the study region, along line AB, was found by multiplying the VEGAS output  
 213 (i.e., a single number representative of the entire study region) by the value of NDVI<sup>GRID BOX</sup> for  
 214 each specific grid box, and dividing by the sum of NDVI<sup>GRID BOX</sup> for all grid boxes. In section

215 3.5.1, we describe the impact of biogenic CO<sub>2</sub> flux on the background CO<sub>2</sub> and the mass balance  
216 calculation.

## 217 **2.5 Mass balance approach and sensitivity analysis**

218 A mass balance approach was used to estimate the emission rate of CO<sub>2</sub> from the Balt-Wash area  
219 and from two local power plants. Under steady wind conditions, the horizontal flux of CO<sub>2</sub>  
220 crossing the vertical plane AB located downwind of an emission source can be considered as an  
221 approximation of the vertical flux of CO<sub>2</sub> over the emission source, while the air parcel was  
222 passing through the source (Trainer et al., 1995; White et al., 1983). A similar approach has been  
223 used in previous studies to estimate fluxes of trace gases such as CO<sub>2</sub>, CH<sub>4</sub>, CO, and NO<sub>x</sub> from  
224 various emission sources (Cambaliza et al., 2014; Heimbürger et al., 2017; Kalthoff et al., 2002;  
225 Karion et al., 2015; O’Shea et al., 2014; Peischl et al., 2016; Salmon et al., 2017, 2018). In this  
226 study, the emission rate of CO<sub>2</sub> ( $F$ , mol/s) was calculated with the following equation:

$$227 \quad F = \int_{z_i}^{z_f} \int_{x_i}^{x_f} ([C]_{x,z} - [C_{bg}]_{x,z}) \cdot U_{x,z} \cdot k_x \, dx dz \quad (1)$$

228 where  $x$  is the horizontal and  $z$  is the vertical location in the plane AB. Variables  $x_i$ ,  $x_f$  and  $z_i$ ,  $z_f$  are  
229 the horizontal and vertical bounds of AB influenced by the emission source of interest,  $[C]$  is the  
230 sampled number density of CO<sub>2</sub>, and  $[C_{bg}]$  is the computed background number density of CO<sub>2</sub>.  
231 Also,  $U$  is the wind speed perpendicular to the aircraft heading and  $k$  is the scaling factor for  $U$ ,  
232 defined as the ratio of the mean  $U$  during transport time over the emission source to the value of  
233  $U$  measured at the downwind flights. A detailed description of each parameter is provided in the  
234 following sections.

### 235 **2.5.1 Background mole fractions of CO<sub>2</sub>**

236 For the Balt-Wash area, background regions within the downwind transects were designated at  
237 northern and southern edges (Krautwurst et al., 2016). Then, the CO<sub>2</sub> background was defined by  
238 fitting a linear regression line to the mole fractions of CO<sub>2</sub> measured at both edges of the  
239 transects (Figure S3b, d, e, g). On 19 and 23 February 2015 the mole fractions of CO<sub>2</sub> measured  
240 between the Washington, D.C. and Baltimore, MD plumes along line AB in Figure 1 were lower  
241 than mole fractions of CO<sub>2</sub> measured at the edges of the downwind transect (Figure S3a, c, f).  
242 Our HYSPLIT transport modeling indicates that elevated CO<sub>2</sub> at the downwind transect edges on  
243 these dates was likely due to power plant plumes transported from either Pennsylvania or West  
244 Virginia (see section 3.2). Therefore, an additional background region, approximately midway  
245 between the Washington, D.C. and Baltimore, MD plumes, was designated for the flights  
246 conducted on 19 and 23 February 2015. For the three flights (UMD-RF4, UMD-RF6, and  
247 Purdue-RF3) conducted on these two days, background CO<sub>2</sub> was determined by fitting two linear  
248 regression lines: one from the southern edge to the midway background flight segment and  
249 another from the midway segment to the northern edge. The background mole fractions of CO<sub>2</sub>  
250 were converted into background number density ( $[C_{bg}]$ ) using in-situ measurements of  
251 temperature and the pressure, for use in Equation (1).

252 The accuracy of our estimate of the background CO<sub>2</sub> mole fraction was evaluated by conducting  
253 a comparison to upwind measurements of CO<sub>2</sub> (Figure 2). For the comparison, the CO<sub>2</sub>  
254 background value defined at each point of every downwind transect was examined for potential  
255 pairing to the upwind measurements of CO<sub>2</sub> conducted for the same flight. Forward HYSPLIT  
256 trajectories were computed every 1 sec of each upwind flight segment, which generally occurred

257 along the line CD in Figure 1. For each forward trajectory, a successful pairing was determined if  
258 a trajectory crossed the downwind transect meeting the following conditions: 1) trajectory  
259 altitude was within the PBL at the crossing time of the downwind track, 2) the crossing time of  
260 the downwind track was within  $\pm 1$  hour of the time the aircraft collected data. The upwind data  
261 were collected in early afternoon for all of the flights, and the downwind sampling occurred on  
262 average 2.5 hours later. Figure 2a shows a comparison of a 10 sec running mean of  $\text{CO}_2$  within  
263 the PBL collected during the upwind portion of the indicated flights versus the background value  
264 of  $\text{CO}_2$  computed for the location at which the trajectory crossed the downwind track. The  
265 excellent agreement between the upwind measurements of  $\text{CO}_2$  and our estimate background  
266  $\text{CO}_2$  (mean and standard deviation of  $0.18 \pm 0.79$  ppm) supports the validity of the carbon  
267 emissions computed using the mass balance approach. We are unable to compare upwind  $\text{CO}_2$  to  
268 the estimate of background for UMD-RF9, because the aircraft flight track did not sample the  
269 composition of the atmosphere along line AD in Figure 1 that corresponds to the upwind location  
270 for this flight, due to the presence of northeasterly winds.

271 Figure 2b compares the depth of the mixed layer, for the upwind flight leg (ordinate) and  
272 downwind flight leg (abscissa). The values originate from the North American Regional  
273 Reanalysis (NARR) meteorological fields for February 2015, because the depth of the PBL from  
274 NARR exhibits the closest agreement with the depth of the PBL inferred from our flight data.  
275 Figure 2 shows considerable variations in both the depth of the PBL and upwind  $\text{CO}_2$ , between  
276 the six flights for which such a comparison is possible. Undoubtedly, this variation in the depth  
277 of the PBL plays a role in value of  $\text{CO}_2$  along the upwind leg. The fact that the depth of the PBL  
278 is stable between the upwind and downwind portions of the flight again supports the validity of  
279 the carbon emissions found using our mass balance approach.

280 For power plant plumes, the horizontal bounds of the plume were determined based on large,  
281 sharp gradients in the in-situ measurements of  $\text{CO}_2$  as shown in Figure 3. The connection of  
282 these enhancements of  $\text{CO}_2$  to local, nearby power plant emissions was confirmed based upon  
283 visual inspection of HYSPLIT back trajectories initialized every 1 s along the flight track, shown  
284 also in Figure 3. The  $\text{CO}_2$  background for power plant plumes was defined as a linear function fit  
285 to the mole fractions of  $\text{CO}_2$ , measured by the Picarro (G2401-m) on board the aircraft, at the  
286 either side of the plume's bounds. All 16 power plant plumes considered below displayed large  
287 enhancements of  $\text{CO}_2$  that could clearly be traced to a local, nearby power plant.

288 **2.5.2 Wind**

289 Recently, a systematic aircraft heading-dependent bias was identified in wind speed and  
 290 direction recorded by the Garmin system onboard the UMD aircraft (Ren et al., 2019). A series  
 291 of bias correction methods was developed and applied to the wind measured by the UMD  
 292 aircraft, utilizing a newly installed differential GPS instrument, NAM4 wind data, and local wind  
 293 profilers. Text S1-3 provides a detailed description on how the systematic bias in the aircraft  
 294 wind measurements was corrected. The wind speed perpendicular to the aircraft heading ( $U$ ) was  
 295 calculated using the wind speed, wind direction, and true track angle of the aircraft measured  
 296 downwind of the emission source of interest. Then, 10 second running means of  $U$  were used for  
 297 the mass balance calculation. For the sensitivity analysis, the standard deviation of  $U$  during the  
 298 downwind transect period was added/subtracted from the original  $U$  for the mass balance  
 299 calculation.

300 From back trajectory analysis of seven mass balance flights (UMD RF4,5,6,8,9, Purdue RF3,4),  
 301 we found that the average air transport time over the Balt-Wash area was  $\sim 5$  hours, given the  
 302 average wind speed of  $\sim 7$  m/s across the study area. However, the value of  $U$  varies across the  
 303 study area, which does have an impact on CO<sub>2</sub> emissions found using the mass balance  
 304 approach. To account for the variability of  $U$  during the transport time of air across the study  
 305 area, a scaling factor  $k$  was estimated in following manner. For each  $0.1^\circ \times 0.1^\circ$  horizontal grid,  
 306 average  $U$  within the PBL (hereafter  $\overline{U_{PBL}}$ ) was derived from NAM4 for the hour closest to the  
 307 mean aircraft observation time (Figure S4a). Then, the resulting values of  $\overline{U_{PBL}}$  were averaged  
 308 within a series of diagonal latitudinal bins across the Balt-Wash study area (Figure S4b). For  
 309 each latitudinal bin, the scaling factor  $k$  was calculated by dividing the mean of all  $\overline{U_{PBL}}$  with the  
 310  $\overline{U_{PBL}}$  at the downwind edge. Obtained  $k$  for latitudinal bins were interpolated and applied to  
 311 individual wind measurements ( $U$ ) (Figure S4c). We found that  $k$  values averaged for each of the  
 312 seven mass balance flights range from 0.75 to 1.06 (Table 1). For the sensitivity analysis,  $k$  was  
 313 calculated using the same method, but for  $\pm 1$  hour from the mean aircraft observation time.  
 314 Then, the standard deviation of  $k$  within three hours span was added/subtracted from the original  
 315  $k$  for the mass balance calculation.

316 To address the impact of the scaling factor  $k$  on our determination of emissions of CO<sub>2</sub> from the  
 317 Balt-Wash area, emissions were also estimated assuming consistent perpendicular wind speed  
 318 throughout the transport time ( $k=1$ ). When consistent wind ( $k=1$ ) is assumed, the monthly total  
 319 FFCO<sub>2</sub> emission was estimated to be 2.0 MtC, which is 5% larger than the estimate of 1.9 MtC  
 320 that accounts for the variability of  $U$  during the air transport time. Further details are given in  
 321 Figures S5 and S6. Given the relatively short transport time of power plant plumes between  
 322 emission and aircraft sampling, the scaling factor  $k=1$  was used for the calculation of power  
 323 plant emissions of CO<sub>2</sub>.

324 **2.5.3 Vertical and horizontal boundary**

325 To include emissions of CO<sub>2</sub> transported above the PBL into our estimate of CO<sub>2</sub> emissions, the  
 326 adjusted mixing height ( $z_{adj}$ ) was determined and used as a vertical bound ( $z_f$ ) of the mass  
 327 balance equation. First, the well-mixed planetary boundary layer height ( $z_{pbl}$ , dashed line in  
 328 Figure S7) and the entrainment height ( $z_e$ , dotted line in Figure S7), an altitude where mixing  
 329 from the PBL has reached free tropospheric level, were determined from the vertical profiles of  
 330 potential temperature and mole fractions of the trace gases (CO<sub>2</sub>, CH<sub>4</sub>, and H<sub>2</sub>O). Then, the

331 adjusted mixing height ( $z_{adj}$ ) was calculated using  $z_{adj} = (3z_{pbl} + z_e) / 4$ , as described by Peischl et  
 332 al. (2016). Also,  $\pm 1\sigma$  uncertainty of  $z_{adj}$  was determined as  $\pm (z_{pbl} - z_e) / 2$  (Figure S7), again  
 333 from Peischl et al. (2016). For flights that obtained multiple vertical profiles (UMD-RF4,5,8 and  
 334 Purdue-RF3,4), the adjusted mixing height and its uncertainty ( $z_{adj} \pm 1\sigma$ ) determined from each  
 335 vertical profile were linearly fit as a function of the observation time. From this function, the  
 336 vertical boundary of the PBL and its uncertainty ( $z_f \pm 1\sigma$ ) were determined at the mid-point of the  
 337 downwind flight period. For the flights with a single vertical profile in the downwind region  
 338 (UMD-RF6,9), values of  $z_{adj}$  and their  $1\sigma$  estimated from the only vertical profile were used to  
 339 define  $z_f \pm 1\sigma$ . For the sensitivity analysis, values of  $z_f \pm 1\sigma$  were used as the vertical boundary in  
 340 the mass balance calculation.

341 Horizontal boundaries ( $x_i, x_f$ ) were determined as the locations where the HYSPLIT back  
 342 trajectory passed through the southern and northern bounds of the Balt-Wash area (UMD-  
 343 RF4,5,6,8 and Purdue-RF3,4). For UMD-RF9, horizontal boundaries were determined as the  
 344 locations where the back trajectory went through the western or southern bound of the study  
 345 area. To estimate the emission rate of CO<sub>2</sub>, horizontal fluxes were calculated for each point in the  
 346 downwind transects (unit: gC m<sup>-2</sup> sec<sup>-1</sup>). The calculated fluxes were averaged into a single value,  
 347 then multiplied by the horizontal ( $x_f - x_i$ ) and vertical boundary distances ( $z_f - z_i$ ) (unit: gC sec<sup>-1</sup>),  
 348 as described by Equation (1).

### 349 **3 Results**

#### 350 **3.1 Source identification and attribution: Baltimore, MD-Washington, D.C. area**

351 During the aircraft campaign, spikes of CO<sub>2</sub> were often observed. For example, for UMD-RF5  
 352 on 20 February 2015, three spikes of CO<sub>2</sub> were recorded downwind of the Balt-Wash area (green  
 353 shaded areas in Figure 3b). To determine the sources of these plumes, a series of HYSPLIT back  
 354 trajectories were calculated. When the wind direction was consistent during the transport over  
 355 the Balt-Wash area, which was the case for 20 February 2015, power plant plumes could be  
 356 clearly isolated from the emissions of the surrounding urban region (Figure 3a). The first two  
 357 spikes of CO<sub>2</sub> observed at 15:40 and 15:47 (EST) were attributed to the Morgantown (MT) and  
 358 Chalk Point (CP) power plants, respectively. The spike of CO<sub>2</sub> observed downwind of the  
 359 Baltimore, MD (16:05) was attributed to the Brandon Shores and H. A. Wagner (B&W) power  
 360 plants, which are in close proximity. According to CEMS records, the B&W, MT, CP power  
 361 plants emitted 1470, 980, 540 tons of CO<sub>2</sub> and 2.8, 0.8, 0.8 tons of SO<sub>2</sub> respectively, during a  
 362 one-hour period from 14:00 PM to 15:00 PM on 20 February 2015. Simultaneous increases of  
 363 the mole fractions of SO<sub>2</sub> for the three spikes of CO<sub>2</sub>, showing ratios of SO<sub>2</sub>/CO<sub>2</sub> mole fraction  
 364 similar to those from CEMS records, confirm that the plumes were emitted from power plants.  
 365 The B&W, MT, and CP power plants emitted total of 3.4 MtC in year 2015, contributing 75.4%  
 366 of the annual total power plant emissions of CO<sub>2</sub> in Maryland (USEPA GHGRP, 2019).

367 Along with the three spikes of CO<sub>2</sub> attributed to local power plants, broad areas of increased CO<sub>2</sub>  
 368 were observed downwind of the Washington, D.C. and Baltimore, MD (grey shaded areas in  
 369 Figure 3b). We argue that increased mole fractions of CO<sub>2</sub> downwind of the Washington, D.C.  
 370 area were mostly induced by emissions from local fossil fuel combustion, while increased CO<sub>2</sub>  
 371 downwind of Baltimore was induced by a mixture of plumes from that city and from several  
 372 power plants in the state of Pennsylvania (See section 3.2).

### 3.2 Source identification and attribution: Inter-state transport of power plant plumes

374 During the aircraft campaign, several spikes in the mole fraction of SO<sub>2</sub> were observed both  
375 upwind and downwind of the Balt-Wash area. To find the sources of these plumes of SO<sub>2</sub>,  
376 HYSPLIT back trajectories were calculated on six days (Figure 4a-f). These trajectories showed  
377 that some of the SO<sub>2</sub> plumes observed downwind of the Balt-Wash area are likely to be the same  
378 plumes observed on the upwind flight legs (Figure 4a, b, d, e). During UMD-RF8, the aircraft  
379 observed a broad increase of SO<sub>2</sub> north of Washington, D.C. due to advection from the westerly  
380 wind direction (Figure 4f). Figure 4g shows that several plumes of SO<sub>2</sub> observed downwind of  
381 the Balt-Wash area were transported from the mid-west Pennsylvania area where five large  
382 power plants are located. The total nameplate capacity of the five power plants was 6,444 MW  
383 (Coal: 90.3% Natural gas: 9.4%) according to USEIA (2016). The Homer City power plant was  
384 reported as one of the largest SO<sub>2</sub> emitting facility in the entire U.S. for 2015 (USEPA AMPD,  
385 2015). As the five power plants are geographically aligned from northwest to southeast in close  
386 proximity, a northwesterly wind is likely to merge the plumes from these power plants, leading  
387 to the inter-state transport of a highly polluted plume with relatively small horizontal width into  
388 the Balt-Wash area.

389 To further investigate the impact of upwind power plant plumes on the aircraft measurements,  
390 forward transport modeling of power plant CO<sub>2</sub> was conducted for 19 and 20 February 2015  
391 (UMD-RF4, 5). Figure 5 shows that airborne observations of the spikes in CO<sub>2</sub>, induced by both  
392 local and upwind power plants, were well reproduced by the forward modeling (HYSPLIT CO<sub>2</sub>).  
393 A contour map of HYSPLIT CO<sub>2</sub> shows that continuous flow of CO<sub>2</sub> from power plants in  
394 Pennsylvania (PA) and West Virginia (WV) sometimes passed through parts of the Balt-Wash  
395 area. According to the HYSPLIT analysis, CO<sub>2</sub> from power plants in PA passed downwind of  
396 Baltimore, MD and accounted for a significant portion of the total amount of CO<sub>2</sub> in the model  
397 grids (27.5% on UMD-RF4 and 35.4% on UMD-RF5). This forward modeling result agrees with  
398 the result from the SO<sub>2</sub> back trajectory analysis, which attributed some plumes of SO<sub>2</sub> observed  
399 downwind of Baltimore, MD to the power plants in PA (Figure 4c, d). However, CO<sub>2</sub> emitted by  
400 power plants in Ohio (OH) was relatively well distributed over a large horizontal distance when  
401 it reached the Balt-Wash area. This result implies that power plant emissions from OH and  
402 farther upwind states would have negligible impact on mass balance calculation for the Balt-  
403 Wash area. The emissions of CO<sub>2</sub> from power plants in PA and WV, however, must be  
404 considered in our analysis.

405 In summary, both the SO<sub>2</sub> back trajectory and CO<sub>2</sub> forward modeling results indicate that inter-  
406 state transport of power plant plumes can induce local increases of the mole fractions of CO<sub>2</sub>  
407 around the Balt-Wash area, especially when consistent northwesterly wind prevails. Accurate  
408 representation of the spatially varying CO<sub>2</sub> background is therefore needed to account for  
409 upwind power plant emissions of CO<sub>2</sub> in the mass flux calculation for the Balt-Wash area.

### 410 3.3 Power plant emissions: Evaluating the aircraft-based mass balance approach

411 Prior to applying the mass balance approach to the Balt-Wash area, the accuracy and precision of  
412 the technique was evaluated using the Continuous Emissions Monitoring Systems (CEMS)  
413 records for CO<sub>2</sub> from two local power plants. Several spikes of CO<sub>2</sub> could be attributed to either  
414 the CP or MT power plant (Figure 3), and were used for the mass balance calculation. The total  
415 uncertainty of the CEMS records was determined by propagating individual uncertainty in the  
416 following terms: volumetric flow rate/CO<sub>2</sub> concentration measurements by CEMS (USEPA,

417 2009), difference of CEMS records against fuel consumption based U.S. Energy Information  
 418 Administration (EIA) datasets (Gurney et al., 2016; Quick & Marland, 2019), and atmospheric  
 419 transport time of power plant plumes. A detailed description of this uncertainty propagation is  
 420 given in Text S4.

421 In Figure 6a, colored symbols show the 16 aircraft-based mass balance estimates of emission  
 422 rates of CO<sub>2</sub> for the CP and MT power plants. The black lines show the hourly emission record  
 423 of each power plant reported to EPA CAMD. According to EPA CAMD, a total of 0.23 MtC was  
 424 emitted by the two power plants during February 2015. Of the total emissions, 98.8% was  
 425 measured directly by CEMS, while 1.2% was either calculated or went through substitution  
 426 procedures. All emissions records during the mass balance flights period were solely from  
 427 CEMS.

428 The mean percentage error (MPE) and the mean absolute percentage error (MAPE) were -0.3%  
 429 and 24%, respectively, for all 16 mass balance estimates the CO<sub>2</sub> emission rate (FLAGG-MD)  
 430 relative to that provided by CEMS (Figure 6b). The mean and standard deviation of the  
 431 difference between the FLAGG-MD and CEMS emission values are  $-5 \pm 43$  tC/hr. However,  
 432 much larger differences, ranging from -58% to 84%, are observed for individual plume sampling  
 433 comparisons. The large variation in these individual relative differences implies that the emission  
 434 rate of CO<sub>2</sub> estimated from a single mass balance experiment may include significant random  
 435 error. Such random error is most likely to be induced by incomplete mixing of power plant  
 436 plumes within the boundary layer, causing the unrepresentative sampling of power plant plumes.  
 437 The CO<sub>2</sub> background, often considered as a significant source of uncertainty in the mass balance  
 438 approach for urban plumes (Cambaliza et al., 2014; Heimbürger et al., 2017; Turnbull et al.,  
 439 2018), is unlikely to be a source of error for power plant plumes given their narrow horizontal  
 440 widths and a large value of the term  $([C] - [C_{bg}])$  that appears in Equation (1) (Figure 3). The  
 441 mean value of  $([C] - [C_{bg}])$  at the peak of the spikes for the 16 sampled plumes was ~5.5 ppm.  
 442 We also found that the combined error for multiple mass balance estimates of power plant  
 443 emissions decreases approximately as the square root of the number of the plume crossings rises,  
 444 which suggests the estimates are indeed influenced by random error. Our analysis suggests that  
 445 power plants emissions can be estimated with MPE of ~10% (or less) when the total number of  
 446 twelve (or more) plumes were sampled by aircraft for the mass balance calculation (95%  
 447 confidence level). The importance of repeating mass balance experiments for the same emission  
 448 source has been discussed in Heimbürger et al. (2017).

### 449 **3.4 The Baltimore, MD-Washington, D.C. area emissions: Sensitivity analysis**

450 The emission rate of CO<sub>2</sub> from the Balt-Wash area was estimated based on the five UMD flights  
 451 and two Purdue flights. Table 1 summarizes the mean and the standard deviation of the five mass  
 452 balance parameters shown in Equation (1) for these seven flights.

453 Table 2 shows the baseline estimates of the emission rate of CO<sub>2</sub> that we consider to be the best  
 454 estimates for the seven research flights. As the experimental period spans nine days in late  
 455 February, the emission rate of CO<sub>2</sub> from the study area may be assumed to be constant during the  
 456 sampling period. This assumption is supported by the fact that the emission rate of CO<sub>2</sub> derived  
 457 from FFDAS shows small variation during the sampling period, having a relative standard  
 458 deviation of 3% (See section 3.5.2). Assuming a constant emission rate, the standard error of the  
 459 mean at 95% confidence level (SEM95) can be calculated as a measure of the precision with the  
 460 following equation:  $\frac{t^* \sigma}{\sqrt{n}}$ , where  $t^*$ -student = 2.306,  $\sigma$  is the sample standard deviation of the seven

461 mass balance estimates, and  $n$  is the number of the mass balance experiments (Heimbürger et al.,  
462 2017). The mean of the seven baseline estimates and its SEM95 were  $89,000 \pm 15,000$  mol/s  
463 ( $3,870 \pm 630$  tC/hr). This result indicates that the emission rate of CO<sub>2</sub> over the Balt-Wash area in  
464 the late February could be determined with the precision of 16% at 95% CL by repeating the  
465 mass balance experiments seven times within a nine day span.

466 The sensitivity of the baseline estimates was tested against the following five parameters:  
467 background CO<sub>2</sub>, PBL height, wind variability observed during the downwind flight, wind  
468 variability during air transport cross the study area, and instrument uncertainty. For the  
469 sensitivity test, the  $\pm 1\sigma$  uncertainty value of each parameter were used for the mass balance  
470 calculation. Section 2.5 describes how the  $1\sigma$  uncertainty was determined for each of these five  
471 parameters. Table 2 shows relative differences (RD) of the newly calculated emission rates  
472 against their baseline estimates.

473 On average, the estimated emission rate of CO<sub>2</sub> is most sensitive to the uncertainty of the  
474 perpendicular wind speed observed during downwind flight, with the mean of the seven RD as  
475  $\pm 25\%$ . The PBL height and the CO<sub>2</sub> background were the second and the third most important  
476 parameters contributing to the overall uncertainty in the emission rate of CO<sub>2</sub>. Instrument  
477 measurement uncertainties (temperature, pressure, CO<sub>2</sub>) and the wind variability during the air  
478 transport over the Balt-Wash area (parameter  $k$ ) show less significant impact the emission  
479 estimate of CO<sub>2</sub> than other parameters.

480 The total uncertainty ( $1\sigma$ ) for each baseline estimate was determined by propagating  $1\sigma$  values of  
481 the five sensitivity parameters using Monte Carlo simulations. The total uncertainty of seven  
482 mass balance estimates ranged from  $\pm 31\%$  to  $\pm 49\%$ , with the mean of the seven total  
483 uncertainties being  $\pm 38\%$ . The precision assigned to the mean of the seven independent mass  
484 balance estimates with SEM95 is  $\pm 16\%$ , which is much lower than the average of the seven total  
485 uncertainties (38%). These results are comparable to findings from previous INFLUX studies  
486 that made use of an aircraft-based mass balance approach to estimate urban CO<sub>2</sub> emissions.  
487 Cambaliza et al. (2014) assigned an overall uncertainty of  $\sim 37\%$  (or conservative  $\sim 50\%$  when  
488 including unknown systematic errors) to the CO<sub>2</sub> emission rate estimated from a single aircraft-  
489 based mass balance experiment. Heimbürger et al. (2017) estimated CO<sub>2</sub> emission rates for the  
490 city of Indianapolis with SEM95 of  $\pm 17\%$  by averaging nine aircraft-based mass balance  
491 estimates conducted during November-December 2014.

### 492 **3.5 Comparison of top-down and bottom-up emissions**

493 In this study, differences between atmospheric observation based (top-down) and inventory data  
494 based (bottom-up) approaches were studied from three different perspectives. First, geographical  
495 distributions of CO<sub>2</sub> flux were compared for five bottom-up products: Anthropogenic Carbon  
496 Emissions System version 1 (ACESv1, (Gately & Hutyra, 2017, 2018)), Emissions Database for  
497 Global Atmospheric Research version 4.3.2 (EDGARv432, (Janssens-Maenhout et al., 2017)),  
498 FFDASv2.2, the Open-Source Data Inventory for Anthropogenic CO<sub>2</sub> version 2018  
499 (ODIAC2018, (Oda et al., 2018; Oda & Maksyutov 2011, 2015)), and CarbonTracker version  
500 2017 (CT2017, (Peters et al., 2007)). Second, hourly emissions of CO<sub>2</sub> estimated from the  
501 aircraft (FLAGG-MD) were compared to hourly emissions from Fossil Fuel Data Assimilation  
502 System version 2.2 (FFDASv2.2, (Asefi-Najafabady et al., 2014; Rayner et al., 2010)). Finally,  
503 monthly emissions of CO<sub>2</sub> estimated from FLAGG-MD were compared to monthly emissions  
504 from the bottom-up products.

505 The bottom-up gridded products were largely developed based upon the emission downscaling  
 506 method, which attempts to downscale national (or sub-national) and annual (or sub-annual)  
 507 emissions inventories into model grids using spatiotemporal metrics (Gurney et al., 2019; Oda et  
 508 al., 2019). For example, ODIAC2018 downscales emissions estimates from the Carbon Dioxide  
 509 Information Analysis Center (CDIAC) into a 1 km global grid, using the carbon monitoring  
 510 action (CARMA) data for power plants and the Defense Meteorological Satellite Program  
 511 (DMSP) nightlight imagery for non-point sources. FFDASv2.2 downscales national emissions  
 512 estimates by the International Energy Agency (IEA) onto a 0.1° resolution lat/lon global grid,  
 513 using data assimilation to combine DMSP nightlight, population, traffic pattern, and power plant  
 514 data. EDGARv432 downscales national sectoral emissions estimates onto a 0.1° lat/lon global  
 515 grid for each emissions sector specified by IPCC. ACESv1 downscales the sector-specific  
 516 emissions estimates provided by the National Emissions Inventory (NEI), Greenhouse Gas  
 517 Reporting Program (GHGRP), and Database of Road Transportation Emissions (DARTE) onto 1  
 518 km spatial resolution U.S. northeast regional grid. CT2017 is a data assimilation system with  
 519 four sectors: fossil fuel combustion, biosphere, ocean, and fire. For the biosphere and ocean  
 520 sectors, prior model CO<sub>2</sub> fluxes were optimized onto a 1° lat/lon global grid using atmospheric  
 521 CO<sub>2</sub> observations and transport simulations. For the fossil fuel combustion sector, emissions  
 522 from ODIAC and the “Miller” emissions data set were averaged onto a 1° lat/lon global grid.  
 523 The net amount of biogenic CO<sub>2</sub> emitted from the Balt-Wash area during February 2015 was  
 524 computed from CT2017, and this value was compared to the VEGAS estimate of the biogenic  
 525 CO<sub>2</sub> emissions (section 3.5.3).

### 526 **3.5.1 The Baltimore, MD-Washington, D.C. area: Spatial distribution of CO<sub>2</sub> flux**

527 Figure 7 shows the spatial distribution of Fossil Fuel CO<sub>2</sub> (FFCO<sub>2</sub>) flux over the Balt-Wash area  
 528 from the five bottom-up products. These five bottom-up emission inventories indicate similar  
 529 overall patterns, but distinctly different geographic distributions of the emissions due to  
 530 variations in the underlying metrics that drive the emissions as well as spatial resolution.  
 531 ACESv1 (with a 1 km resolution) shows highly resolved geographical distributions of FFCO<sub>2</sub>,  
 532 such as the Beltway around Washington, D.C. and I-95 highway connecting major cities in the  
 533 northeast corridor, due to their use of census block-level geospatial information (Gately &  
 534 Hutyra, 2017). ODIAC2018, also at 1 km resolution, does not resolve individual roads due to  
 535 their use of satellite-observed nighttime light data as a spatial emission proxy for non-point  
 536 source emissions (Oda et al., 2018; Oda & Maksyutov, 2011). Still, it is noticeable that the  
 537 global model ODIAC2018 shows a horizontal transect of CO<sub>2</sub> flux summed across the study area  
 538 that is similar to that from the regional model ACESv1 (Figure 7f). The difference between  
 539 ACESv1 and ODIAC2018 emissions would be less significant at an aggregated coarser spatial  
 540 resolution, such as the resolution of the many inverse model simulations (Oda et al., 2019). Maps  
 541 of CO<sub>2</sub> flux from FFDASv2.2 and EDGARv432 (0.1° resolution) show emission hot spots for  
 542 the major power plants and the urban areas. Emissions from these power plants are represented  
 543 by the higher resolution ACESv1 and ODIAC2018 inventories, but are difficult to see on panels  
 544 (a) and (b) of Figure 7 because the pixels are so small. Horizontal transects of the CO<sub>2</sub> flux  
 545 derived from FFDASv2.2 and EDGARv432 exhibit an overall similar shape to those from  
 546 ACESv1 and ODIAC2018, while spikes induced by power plants are more apparent in the flux  
 547 transects from ACESv1 and ODIAC2018 due to higher spatial resolution (Figure 7f). The  
 548 CT2017 inventory has a 1° lat/lon resolution, and hence the CT2017 map of FFCO<sub>2</sub> is more

549 spatially uniform at the scale of our study domain, since there are only 4 grid cells covering the  
550 Balt-Wash area.

551 According to VEGAS, the net amount of CO<sub>2</sub> emitted by the biogenic sector was ~0.4 MtC in  
552 the Balt-Wash area during February 2015. However, the horizontal transect of biogenic CO<sub>2</sub>,  
553 simulated by VEGAS and scaled by NDVI (see section 2.4), is nearly constant across the Balt-  
554 Wash area during February 2015 (Figure 7f). This horizontal transect for biogenic emissions  
555 across our study area indicates that the CO<sub>2</sub> background, defined by the linear fitting method, is  
556 likely to already include the enhancement signal due to biogenic emissions. Therefore, we did  
557 not attribute any of the CO<sub>2</sub> flux found from the mass balance estimate to the biogenic sector  
558 (Figure 8). We acknowledge that the lack of any independent source of validation for  
559 VEGAS/NDVI outputs, such as radiocarbon measurements or eddy covariance flux towers,  
560 might be a weakness in our analysis. On-going efforts to develop <sup>13</sup>CO<sub>2</sub> and radiocarbon  
561 measurements from NIST northeast corridor tower network (Karion et al., 2019) and urban  
562 biospheric CO<sub>2</sub> models (Hardiman et al., 2017; Smith et al., 2019) will provide further  
563 opportunity to study the impact of biogenic CO<sub>2</sub> flux on the aircraft-based mass balance  
564 estimates.

### 565 **3.5.2 Hourly emission rate of CO<sub>2</sub> from the Baltimore, MD-Washington, D.C. area**

566 The FLAGG-MD estimate of fossil-fuel combustion CO<sub>2</sub> (FFCO<sub>2</sub>) emission rate is derived from  
567 the baseline mass balance estimates shown in Table 2. First, the emissions of CO<sub>2</sub> from  
568 human/pet respiration (human, dog, and cat) are estimated based on the following assumptions:  
569 the population in the Balt-Wash study area (red box, Figure 7e) was ~8.1 million in February  
570 2015 (CIESIN, 2018); the CO<sub>2</sub> release rate by human respiration is 254 gC/person/day (Prairie &  
571 Duarte, 2007); dog/cat ownership is 0.22 dogs/person and 0.24 cats/person, and the dog/cat  
572 release rate of CO<sub>2</sub> is 25% of the human release rate (American Veterinary Medical Association,  
573 2012). Next, the estimated emissions from human/pet respiration are subtracted from the baseline  
574 mass balance estimates. Then, the remainder of the mass balance estimates was apportioned to  
575 either FFCO<sub>2</sub> or Non-FFCO<sub>2</sub> Anthropogenic emissions (hereafter ‘NFA-CO<sub>2</sub>’) by applying the  
576 ratio derived from the Maryland GHG inventory for year 2014 (MDE, 2016). The NFA-CO<sub>2</sub>  
577 consists of following sectors: 1) industrial processes (cement manufacture, limestone and  
578 dolomite, soda ash, ammonia and urea production), 2) agriculture (urea fertilizer usage), 3) waste  
579 management (waste combustion, landfills, and residential open burning). Note that emissions  
580 from gasoline for on-road transportation were solely regarded as FFCO<sub>2</sub>, as the emissions from  
581 ethanol (E85) in gasoline comprises only ~0.1% of total emissions from gasoline for on-road  
582 transportation (MDE, 2016). See Text S5 for a detailed description of the method utilized for  
583 human/pet respiration and the FFCO<sub>2</sub> to Non-FFCO<sub>2</sub> ratio from the Maryland GHG inventory,  
584 and their associated uncertainties. Note that we did not apportion any of the mass balance  
585 estimates to the biogenic sector, as discussed in section 3.5.1.

586 Figure 8 shows the emission rates of CO<sub>2</sub> from the Balt-Wash area estimated from seven  
587 FLAGG-MD flights and corresponding FFDASv2.2 estimates. On average, FFCO<sub>2</sub> comprises  
588 93% of the mass balance estimates, while NFA-CO<sub>2</sub> and human/pet respiration comprises 4.6%  
589 and 2.6%, respectively. Overall, the emission rate of FFCO<sub>2</sub> from FFDASv2.2 for the flight days  
590 was 32% larger than that from FLAGG-MD but within the 1 $\sigma$  uncertainty range for most flights,  
591 except UMD-RF5. Still, such level of agreement is very meaningful given that FLAGG-MD and

592 FFDASv2.2 use two independent approaches: aircraft observation-based sampling versus a data  
593 assimilation framework for disaggregating the annual/national inventory into hourly/0.1° grids.

594 Turnbull et al. (2018) highlighted that the background CO<sub>2</sub>, determined from the edge fitting  
595 method, is likely to be overestimated when there are nonzero emissions over the edge region of  
596 the study domain. In their study, CO<sub>2</sub> flux values were computed using an approach similar to  
597 Equation (1). Then, computed CO<sub>2</sub> flux values were scaled to a background-corrected aircraft  
598 mass balance flux by adding a mean CO<sub>2</sub> flux value for the rural area outside the aircraft  
599 footprint which was determined from a bottom-up inventory. Should we take the same approach,  
600 using either FFDAS or ODIAC to define the emissions of CO<sub>2</sub> along the narrow vertical boxes  
601 that define region illustrated in Figure 7, our value of FFCO<sub>2</sub> for the Balt-Wash area would  
602 increase by 30%, rising from 1.9 MtC to 2.5 MtC. This type of adjustment is not used in our  
603 analysis for two reasons. First, this adjustment implicitly assumes our estimate of background  
604 CO<sub>2</sub> is too large by approximately 0.3 ppm, whereas the comparison of the mole fraction of  
605 background CO<sub>2</sub> to the measured upwind mole fraction of CO<sub>2</sub> already indicates a potential bias  
606 of 0.18 ppm (Figure 2a). If we were to adjust background CO<sub>2</sub> to adjust for possible  
607 unaccounted emissions in these edge, rectangular regions, the scatter plot between upwind and  
608 background CO<sub>2</sub> would exhibit such a bias that would begin to approach the standard deviation  
609 of the difference between upwind and background CO<sub>2</sub>. Second, this adjustment assumes that  
610 anthropogenic emissions of CO<sub>2</sub> can be well defined in sparsely populated geographic regions by  
611 global models. We are reluctant therefore to make such an adjustment to our estimate of FFCO<sub>2</sub>  
612 for the Balt-Wash area, but we acknowledge that our definition of background CO<sub>2</sub> found using  
613 the method illustrated in Figure S3 could potentially need revision, due to lack of explicit  
614 consideration of anthropogenic emissions of CO<sub>2</sub> in these edge regions. Our approach is similar  
615 to the methodology used in numerous other recent mass balance studies (Heimbürger et al.,  
616 2017; Krautwurst et al., 2016; Ren et al., 2019).

617 Finally, we acknowledge that the rectangular-shaped region (Figure 7), determined based on the  
618 dominant wind direction, may not perfectly represent the emissions area that induced enhanced  
619 CO<sub>2</sub> observed by the aircraft, especially when uncertainties associated with wind variability  
620 determination are significant. Such mis-representation of the emissions area could have  
621 potentially contributed to the difference between top-down and bottom-up estimates (Lopez-Coto  
622 et al., 2020; Turnbull et al., 2018). In this study, flight-by-flight adjustment for the geographic  
623 study area was not attempted, as six of the seven flights share similar flight patterns and wind  
624 conditions. Unlike the other flights, UMD-RF9 was conducted under northeasterly wind  
625 conditions.

### 626 **3.5.3 Monthly total emission of CO<sub>2</sub> from the Baltimore, MD-Washington, D.C. area**

627 The four bottom-up gridded products cover different years (i.e., EDGARv432: 2010, ACESv1:  
628 2014, FFDASv2.2 and ODIAC2018: 2015) with varying temporal resolution (i.e., EDGARv432  
629 and ODIAC2018: monthly, FFDASv2.2 and ACESv1: hourly). To facilitate the comparison  
630 among these bottom-up models and our mass balance estimates, the amounts of FFCO<sub>2</sub> emitted  
631 during the month of February in the Balt-Wash study area were computed from each bottom-up  
632 product and our seven mass balance estimates shown in Figure 8. No further attempts were made  
633 to harmonize the temporal mismatch existing in EDGARv432 (year 2010) and ACES v1 (year  
634 2014). The FLAGG-MD monthly total FFCO<sub>2</sub> emission was estimated by temporally scaling up  
635 the seven FLAGG-MD emission rates of FFCO<sub>2</sub>, shown in Figure 8. The Temporal

636 Improvements for Modeling Emissions by Scaling (TIMES), which provides scaling factors for  
637 diurnal and weekly variability of FFCO<sub>2</sub> in global rectangular 0.25° lat/lon grids, was used for  
638 the temporal scaling process (Nassar et al., 2013). The monthly emissions from human/pet  
639 respiration and NFA-CO<sub>2</sub> were estimated as described in section 3.5.2. The major challenge for  
640 comparing different bottom-up gridded products is to harmonize various emission source sectors  
641 covered by each product (Gately & Hutyra, 2017; Gurney et al., 2019; Oda et al., 2019). In this  
642 study, source sector harmonizing was only conducted for EDGARv432 (see Text S6), while all  
643 available sectors in other bottom-up products (ACESv1, FFDASv2.2, and ODIAC2018) were  
644 used to derive FFCO<sub>2</sub> emissions. Thus, sectoral mismatching among the FLAGG-MD estimate  
645 and the four bottom-up products exists for the following sectors: cement manufacturing, gas  
646 flaring, aviation, and oil and gas extraction, refining, and transport. These mismatching sectors  
647 account for ~4% of the total FFCO<sub>2</sub> in our study domain (see Text S6). Note that one of the main  
648 objectives set for developing these global bottom-up gridded products was to provide a prior CO<sub>2</sub>  
649 flux for use in inversion modeling (Oda et al., 2018). Therefore, FFCO<sub>2</sub> flux values at specific  
650 time-space model grids should be regarded as a climatological mean rather than snapshot of the  
651 truth (Gurney 2018).

652 We estimate that 2.4 MtC of CO<sub>2</sub> was emitted from the Balt-Wash area during February 2015,  
653 according to the FLAGG-MD estimate (all emission other than biogenic) and VEGAS  
654 simulations (biogenic CO<sub>2</sub>) (Figure 9). The total 2.4 MtC consists of 1.9 MtC of FFCO<sub>2</sub> (78% of  
655 the total), 0.4 MtC of biogenic CO<sub>2</sub> (15%), 0.1 MtC of NFA-CO<sub>2</sub> (4%), and 0.06 MtC of  
656 human/pet respiration (3%). The mean and the standard deviation of the four bottom-up  
657 estimates of FFCO<sub>2</sub> were 2.2±0.3 MtC (FFDASv2.2: 2.5 MtC, ACESv1: 2.3 MtC, EDGARv432:  
658 2.0 MtC, ODIAC2018: 1.9 MtC), which is 15% larger than the FLAGG-MD estimate of FFCO<sub>2</sub>  
659 (1.9±0.3 MtC). The ODIAC2018 bottom-up estimate of FFCO<sub>2</sub> shows best agreement with the  
660 top-down FLAGG-MD estimate.

661 ACESv1 and EDGARv432 provide sectoral emissions of FFCO<sub>2</sub> for years 2014 and 2010,  
662 respectively. Based on ACESv1, power plant emissions were 24% of the monthly total FFCO<sub>2</sub>,  
663 while they were 35% of the monthly total FFCO<sub>2</sub> according to EDGARv432 (Figure 9).  
664 Estimates from EPA CAMD and FLAGG-MD for our study area suggest power plant emissions  
665 accounted for 29% of the monthly total FFCO<sub>2</sub> emissions in February 2015. On-road  
666 transportation emissions account for 36% of the ACESv1 estimate, while they only account for  
667 13% of the EDGARv432 estimate. A significant difference of on-road emissions between  
668 ACESv1 and EDGARv432 might be due to the temporal mismatching (i.e., 2010 versus 2014) of  
669 the two inventories, but more likely reflects a bias in either one or perhaps both products. Gately  
670 et al. (2013) and McDonald et al. (2014) reported that EDGAR overestimates urban vehicles  
671 emissions in major U.S. cities. However, the recent update of EDGAR version 4.3.2 addressed  
672 this issue by adopting proxy layers for various roads and vehicles types (Janssens-Maenhout et  
673 al., 2017). We have not attempted to further quantify the source of the difference between on-  
674 road emissions of CO<sub>2</sub> for these two inventories, as this effort is beyond the scope of this study.  
675 We leave the detailed analysis of sectoral composition of urban FFCO<sub>2</sub> for future work.

676 We would like to emphasize that this study provides an independent, objective measure for the  
677 emission comparison. Evaluation of downscaled emissions is often difficult mainly due to the  
678 lack of physical measurements (Andres et al., 2016; Oda et al., 2018) and often done by inter-  
679 comparison of emission inventories that allow only for characterization of differences among

680 inventories. This study demonstrates the use of atmospheric measurements for examining the  
681 errors and biases in the emission inventories.

682 Finally, we compare ODIAC2018, which showed the best agreement against our aircraft-based  
683 estimate of the monthly CO<sub>2</sub> emissions, to the Maryland GHG inventory published by the  
684 Maryland Department of the Environment (MDE) (MDE, 2016). The Maryland GHG inventory  
685 estimated that 18.8 MtC of FFCO<sub>2</sub> was emitted from Maryland during year 2014, while  
686 ODIAC2018 estimated 20.2 MtC for the same domain in 2014. The overall excellent agreement  
687 among the top-down approach, bottom-up models, and State emission inventory is promising  
688 given the fact that each relies on independent datasets and methodologies.

#### 689 **4 Conclusions**

690 The first FLAGG-MD aircraft campaign was conducted during February 2015 to study the  
691 emissions of CO<sub>2</sub> in the Balt-Wash area. Several conclusions are drawn from this study.

692 First, a series of HYSPLIT transport modeling analyses was conducted to provide source  
693 attribution of the plumes of CO<sub>2</sub> observed by the aircraft. A number of plumes of CO<sub>2</sub> could be  
694 attributed to either Washington, D.C. and Baltimore, MD, or the major power plants in the study  
695 area. We found that inter-state transport of power plant plumes can induce a substantial local  
696 increase of CO<sub>2</sub> throughout the Balt-Wash area, increasing the spatial variability of background  
697 CO<sub>2</sub>.

698 Second, the accuracy and precision of the aircraft-based mass balance approach were tested  
699 against local power plant emissions, and also the sensitivity of the approach was tested for urban  
700 emissions. Emissions of CO<sub>2</sub> from two local power plants were estimated using aircraft data and  
701 the resulting estimates were found to have no discernible systematic bias, with a mean  
702 percentage error of -0.3 % compared to corresponding CEMS data for 16 cases. Also, power  
703 plants emissions could be estimated with MPE of ~10% when a total number of twelve plumes  
704 was sampled by the aircraft for the mass balance calculation (95% CL). These results  
705 demonstrate that the accuracy of mass balance estimates increases and as the number of mass  
706 balance experiments increases for the same target emission source (Heimbürger et al., 2017;  
707 Karion et al., 2015). From a sensitivity analysis, we found that the variability of the wind speed  
708 and direction downwind of the study area have the largest impact on the mass balance  
709 calculation, followed by the boundary layer height and the specification of background CO<sub>2</sub>. The  
710 1 $\sigma$  uncertainty of a single mass balance estimate of CO<sub>2</sub> emission from the Balt-Wash study area  
711 can be significant, ranging from  $\pm 31\%$  to  $\pm 49\%$ . However, we also found that the precision  
712 assigned to the mean of the seven mass balance estimates was considerably better, with a SEM95  
713 of  $\pm 16\%$ . This result supports the findings from previous studies: the precision of the mass  
714 balance estimate of CO<sub>2</sub> emissions over urban regions is improved by repeating mass balance  
715 experiments numerous times, within a short span of time.

716 Finally, differences among the five bottom-up models (ACESv1, CT2017, EDGARv432,  
717 FFDASv2.2, and ODIAC2018) and the top-down estimate were studied from the perspective of  
718 both the geographical distribution of CO<sub>2</sub> flux and the total emissions over the Balt-Wash study  
719 area. With respect to the geographical distribution of CO<sub>2</sub>, we found that horizontal transects of  
720 CO<sub>2</sub> flux across the Balt-Wash area derived from four models (ACESv1, ODIAC2018,  
721 EDGARv432, and FFDASv2.2) have similar structures, showing spikes for the area where major  
722 power plants and highly developed areas are located. Only ACESv1 provided spatial distribution

723 of CO<sub>2</sub> flux on the spatial scale of individual roads. From the perspective of total monthly  
724 emissions, the FLAGG-MD aircraft flights yield and estimated  $1.9\pm 0.3$  MtC as the amount of  
725 FFCO<sub>2</sub> emitted from the Balt-Wash area during February 2015, and the four bottom-up models  
726 (except for CT2017) estimated  $2.2\pm 0.3$  MtC. ODIAC2018, which provides downscaled  
727 emissions for year 2015, shows best agreement with the FLAGG-MD top-down estimate.  
728 Evaluation of subnational emissions of bottom-up models is often limited to an evaluation based  
729 on an inter-comparison among different models. This study provided an independent, objective  
730 measure for the inventory evaluation. Additionally, we found that the statewide annual total  
731 FFCO<sub>2</sub> emissions in the Maryland (MDE) GHG inventory was 7% lower than the ODIAC2018  
732 estimate.

733 Numerous efforts are currently underway to better understand urban emissions of CO<sub>2</sub>. For  
734 instance, the recent installations of observation towers and low-cost sensors around the Balt-  
735 Wash area will provide improved constraints on spatio-temporal variability of the CO<sub>2</sub>  
736 background (Lopez-Coto et al., 2017; Martin et al., 2017, 2019; Mueller et al., 2018). Also,  
737 radiocarbon measurements and urban-specific biospheric CO<sub>2</sub> models will provide better  
738 understanding on the impact of biogenic CO<sub>2</sub> flux on the aircraft-based mass balance approach.  
739 A new version of VEGAS currently under development will incorporate an accurate  
740 representation of the diurnal cycle of the biogenic flux of CO<sub>2</sub>. Lastly, frequent and regular  
741 aircraft campaigns in the future will provide resources to better understand the gaps among top-  
742 down approaches, bottom-up models, and state/local GHG inventories, benefiting both stake  
743 holders and the carbon cycle modeling community.

744

#### 745 **Acknowledgments, Samples, and Data**

746 The FLAGG-MD project was funded and supported by NIST's Greenhouse Gas Measurements  
747 program. All aircraft observations dataset used in this study are available at  
748 <https://www2.atmos.umd.edu/~flaggmd/>; CarbonTracker CT2017 results provided by NOAA  
749 ESRL, Boulder, Colorado, USA from the website at <http://carbontracker.noaa.gov>. The version  
750 of the ODIAC emission data product (ODIAC2018) is available from the Global Environmental  
751 Database hosted by the Center for Global Environmental Research (CGER), National Institute  
752 for Environmental Studies (NIES), Japan (<http://db.cger.nies.go.jp/dataset/ODIAC/>). Tomohiro  
753 Oda is supported by the NASA Carbon Cycle Science Program (grant no. NNX14AM76G). The  
754 version of ACES emission data (ACESv1) is available through the Oak Ridge National  
755 Laboratory (ORNL) Distributed Active Archive Center (DAAC). The version of the EDGAR  
756 emission data (EDGARv4.3.2) is available at <http://edgar.jrc.ec.europa.eu/overview.php?v=432>  
757 (DOI: [https://data.europa.eu/doi/10.2904/JRC\\_DATASET\\_EDGAR](https://data.europa.eu/doi/10.2904/JRC_DATASET_EDGAR)). Power plants emissions  
758 dataset (Air Markets Program Data) used in this study is available from U.S. EPA AMPD  
759 website (<https://ampd.epa.gov/ampd/>). The authors are grateful to Wenze Yang at NOAA for  
760 providing NDVI (v1r12) data. We are also grateful for numerous helpful discussions with Anna  
761 Karion at NIST. Finally, we sincerely appreciate the helpful comments provided by Jocelyn  
762 Turnbull and an anonymous reviewer to the original submitted manuscript.

#### 763 **Disclaimer**

764 Certain commercial equipment, instruments, or materials are identified in this paper in order to  
765 specify the experimental procedure adequately. Such identification is not intended to imply  
766 recommendation or endorsement by the National Institute of Standards and Technology, nor is it

767 intended to imply that the materials or equipment identified are necessarily the best available for  
768 the purpose.

## 769 **References**

- 770 American Veterinary Medical Association. (2012). U.S. Pet ownership statistics. Retrieved  
771 September 7, 2019, from [https://www.avma.org/KB/Resources/Statistics/Pages/Market-](https://www.avma.org/KB/Resources/Statistics/Pages/Market-research-statistics-US-pet-ownership.aspx)  
772 [research-statistics-US-pet-ownership.aspx](https://www.avma.org/KB/Resources/Statistics/Pages/Market-research-statistics-US-pet-ownership.aspx)
- 773 Andres, R. J., Boden, T. A., & Higdon, D. M. (2016). Gridded uncertainty in fossil fuel carbon  
774 dioxide emission maps, a CDIAC example. *Atmospheric Chemistry and Physics*, *16*(23).  
775 <https://doi.org/10.5194/acp-16-14979-2016>
- 776 Asefi-Najafabady, S., Rayner, P. J., Gurney, K. R., McRobert, A., Song, Y., Coltin, K., et al.  
777 (2014). A multiyear, global gridded fossil fuel CO<sub>2</sub> emission data product: Evaluation and  
778 analysis of results. *Journal of Geophysical Research: Atmospheres*, *119*(17), 10,210-  
779 213,231. <https://doi.org/10.1002/2013JD021296>
- 780 Bréon, F. M., Broquet, G., Puygrenier, V., Chevallier, F., Xueref-Remy, I., Ramonet, M., et al.  
781 (2015). An attempt at estimating Paris area CO<sub>2</sub> emissions from atmospheric concentration  
782 measurements. *Atmos. Chem. Phys.*, *15*(4), 1707–1724. [https://doi.org/10.5194/acp-15-](https://doi.org/10.5194/acp-15-1707-2015)  
783 [1707-2015](https://doi.org/10.5194/acp-15-1707-2015)
- 784 Cambaliza, M. O. L., Shepson, P. B., Caulton, D. R., Stirm, B., Samarov, D., Gurney, K. R., et al.  
785 (2014). Assessment of uncertainties of an aircraft-based mass balance approach for  
786 quantifying urban greenhouse gas emissions. *Atmospheric Chemistry and Physics*, *14*(17),  
787 9029–9050. <https://doi.org/10.5194/acp-14-9029-2014>
- 788 CIESIN (Center for International Earth Science Information Network), C. U. (2018). Gridded  
789 population of the world, version 4 (GPWv4): Population count, revision 11.  
790 <https://doi.org/10.7927/H4JW8BX5>
- 791 Davis, K. J., Deng, A., Lauvaux, T., Miles, N. L., Richardson, S. J., Sarmiento, D. P., et al.  
792 (2017). The Indianapolis Flux Experiment (INFLUX): A test-bed for developing urban  
793 greenhouse gas emission measurements. *Elem Sci Anth*, *5*(0), 21.  
794 <https://doi.org/10.1525/elementa.188>
- 795 DOE (Department of Energy & Environment). (2018). Clean Energy DC. Retrieved April 10,  
796 2019, from <https://doee.dc.gov/cleanenergydc>
- 797 Draxler, R., Hess, G. D., & Air Resources Laboratory (U.S.). (1997). Description of the  
798 HYSPLIT\_4 modeling system. Retrieved January 17, 2019, from  
799 <https://www.arl.noaa.gov/documents/reports/arl-224.pdf>
- 800 Draxler, R., Stunder, B., Rolph, G., Stein, A., & Taylor, A. (2014). HYSPLIT4 user 's guide  
801 version 4 - Last revision: September 2014. NOAA. Retrieved from  
802 [https://www.arl.noaa.gov/data/web/models/hysplit4/win95/user\\_guide.pdf](https://www.arl.noaa.gov/data/web/models/hysplit4/win95/user_guide.pdf)
- 803 Duren, R. M., & Miller, C. E. (2012). Measuring the carbon emissions of megacities. *Nature*  
804 *Climate Change*, *2*(8), 560–562. <https://doi.org/10.1038/nclimate1629>
- 805 Feng, S., Lauvaux, T., Newman, S., Rao, P., Ahmadov, R., Deng, A., et al. (2016). Los Angeles  
806 megacity: a high-resolution land–atmosphere modelling system for urban CO<sub>2</sub> emissions.  
807 *Atmos. Chem. Phys.*, *16*(14), 9019–9045. <https://doi.org/10.5194/acp-16-9019-2016>
- 808 Gately, C., & Hutyra, L. (2017). Large uncertainties in urban-scale carbon emissions. *Journal of*  
809 *Geophysical Research: Atmospheres*, *122*(20). <https://doi.org/10.1002/2017JD027359>
- 810 Gately, C., & Hutyra, L. (2018). CMS: CO<sub>2</sub> Emissions from Fossil Fuels Combustion, ACES  
811 Inventory for Northeastern USA. ORNL DAAC, Oak Ridge, Tennessee, USA. ORNL  
812 Distributed Active Archive Center. <https://doi.org/10.3334/ornldaac/1501>

- 813 Gately, C. K., Hutyra, L. R., Wing, I. S., & Brondfield, M. N. (2013). A bottom up approach to  
 814 on-road CO<sub>2</sub> emissions estimates: Improved spatial accuracy and applications for regional  
 815 planning. *Environmental Science & Technology*, 47(5), 2423–2430.  
 816 <https://doi.org/10.1021/es304238v>
- 817 Gratani, L., & Varone, L. (2005). Daily and seasonal variation of CO<sub>2</sub> in the city of Rome in  
 818 relationship with the traffic volume. *Atmospheric Environment*, 39(14), 2619–2624.  
 819 <https://doi.org/10.1016/j.atmosenv.2005.01.013>
- 820 Gurney, K. (2018). Read me file of Hestia fossil fuel farbon dioxide (FFCO<sub>2</sub>) data product - Salt  
 821 lake county, version 2.2, 0.002 degree grid. Retrieved May 10, 2019, from  
 822 <https://data.nist.gov/od/ds/696FD547910012A0E0532457068160E41910/readme.002deg.S>  
 823 [LC.v2.2.txt](https://data.nist.gov/od/ds/696FD547910012A0E0532457068160E41910/readme.002deg.S)
- 824 Gurney, K., Liang, J., Patarasuk, R., O’Keeffe, D., Huang, J., Hutchins, M., et al. (2017).  
 825 Reconciling the differences between a bottom-up and inverse-estimated FFCO<sub>2</sub> emissions  
 826 estimate in a large US urban area. *Elem Sci Anth*, 5. <https://doi.org/10.1525/elementa.137>
- 827 Gurney, K. R., Huang, J., & Coltin, K. (2016). Bias present in US federal agency power plant  
 828 CO<sub>2</sub> emissions data and implications for the US clean power plan. *Environmental Research*  
 829 *Letters*, 11(6), 64005. <https://doi.org/10.1088/1748-9326/11/6/064005>
- 830 Gurney, K. R., Liang, J., O’Keeffe, D., Patarasuk, R., Hutchins, M., Huang, J., et al. (2019).  
 831 Comparison of global downscaled versus bottom-up fossil fuel CO<sub>2</sub> emissions at the urban  
 832 scale in four US urban areas. *Journal of Geophysical Research: Atmospheres*, 124(5),  
 833 2823–2840. <https://doi.org/10.1029/2018JD028859>
- 834 Hardiman, B. S., Wang, J. A., Hutyra, L. R., Gately, C. K., Getson, J. M., & Friedl, M. A. (2017).  
 835 Accounting for urban biogenic fluxes in regional carbon budgets. *Science of the Total*  
 836 *Environment*, 592, 366–372. <https://doi.org/10.1016/j.scitotenv.2017.03.028>
- 837 Heimbürger, A. M. F., Harvey, R. M., Shepson, P. B., Stirn, B. H., Gore, C., Turnbull, J., et al.  
 838 (2017). Assessing the optimized precision of the aircraft mass balance method for  
 839 measurement of urban greenhouse gas emission rates through averaging. *Elem Sci Anth*, 5.  
 840 <https://doi.org/10.1525/elementa.134>
- 841 Hutyra, L. R., Duren, R., Gurney, K. R., Grimm, N., Kort, E. A., Larson, E., & Shrestha, G.  
 842 (2014). Urbanization and the carbon cycle: Current capabilities and research outlook from  
 843 the natural sciences perspective. *Earths Future*, 2(10), 473–495.  
 844 <https://doi.org/10.1002/2014ef000255>
- 845 Idso, C. D., Idso, S. B., & Balling Jr, R. C. (2001). An intensive two-week study of an urban CO<sub>2</sub>  
 846 dome in Phoenix, Arizona, USA. *Atmospheric Environment*, 35(6), 995–1000.  
 847 [https://doi.org/10.1016/S1352-2310\(00\)00412-X](https://doi.org/10.1016/S1352-2310(00)00412-X)
- 848 Janssens-Maenhout, G., Crippa, M., Guizzardi, D., Muntean, M., Schaaf, E., Dentener, F., et al.  
 849 (2017). EDGAR v4.3.2 Global atlas of the three major greenhouse gas emissions for the  
 850 period 1970–2012. *Earth Syst. Sci. Data Discuss.*, 2017, 1–55. <https://doi.org/10.5194/essd->  
 851 [2017-79](https://doi.org/10.5194/essd-2017-79)
- 852 Kalthoff, N., Corsmeier, U., Schmidt, K., Kottmeier, C., Fiedler, F., Habram, M., & Slemr, F.  
 853 (2002). Emissions of the city of Augsburg determined using the mass balance method.  
 854 *Atmospheric Environment*, 36, S19–S31. [https://doi.org/10.1016/S1352-2310\(02\)00215-7](https://doi.org/10.1016/S1352-2310(02)00215-7)
- 855 Karion, A., Sweeney, C., Kort, E. A., Shepson, P. B., Brewer, A., Cambaliza, M., et al. (2015).  
 856 Aircraft-based estimate of total methane emissions from the Barnett shale region.  
 857 *Environmental Science & Technology*, 49(13), 8124–8131.  
 858 <https://doi.org/10.1021/acs.est.5b00217>

- 859 Karion, A., Callahan, W., Stock, M., Prinzivalli, S., Verhulst, K. R., Kim, J., et al. (2019).  
 860 Greenhouse gas observations from the Northeast Corridor tower network. *Earth Syst.*  
 861 *Sci. Data Discuss.*, 2019, 1–29. <https://doi.org/10.5194/essd-2019-206>
- 862 Krautwurst, S., Gerilowski, K., Jonsson, H. H., Thompson, D. R., Kolyer, R. W., Thorpe, A. K.,  
 863 et al. (2016). Methane emissions from a Californian landfill, determined from airborne  
 864 remote sensing and in-situ measurements. *Atmos. Meas. Tech. Discuss.*, 2016, 1–33.  
 865 <https://doi.org/10.5194/amt-2016-391>
- 866 Lauvaux, T., Miles, N. L., Deng, A., Richardson, S. J., Cambaliza, M. O., Davis, K. J., et al.  
 867 (2016). High-resolution atmospheric inversion of urban CO<sub>2</sub> emissions during the dormant  
 868 season of the Indianapolis Flux Experiment (INFLUX). *Journal of Geophysical Research:*  
 869 *Atmospheres*, 121(10), 5213–5236. <https://doi.org/10.1002/2015JD024473>
- 870 Lopez-Coto, I., Ghosh, S., Prasad, K., & Whetstone, J. (2017). Tower-based greenhouse gas  
 871 measurement network design—The National Institute of Standards and Technology North  
 872 East Corridor Testbed. *Advances in Atmospheric Sciences*, 34(9), 1095–1105.  
 873 <https://doi.org/10.1007/s00376-017-6094-6>
- 874 Lopez-Coto, I., Ren, X., Salmon, O. E., Karion, A., Shepson, P. B., Dickerson, R. R., et al.  
 875 (2020). Wintertime CO<sub>2</sub>, CH<sub>4</sub> and CO emissions estimation for the Washington  
 876 DC/Baltimore metropolitan area using an inverse modeling technique. *Environmental*  
 877 *Science & Technology*. <https://doi.org/10.1021/acs.est.9b06619>
- 878 Martin, C. R., Zeng, N., Karion, A., Dickerson, R. R., Ren, X., Turpie, B. N., & Weber, K. J.  
 879 (2017). Evaluation and enhancement of a low-cost NDIR CO<sub>2</sub> sensor. *Atmos. Meas. Tech.*  
 880 *Discuss.*, 2017, 1–25. <https://doi.org/10.5194/amt-2016-396>
- 881 Martin, C. R., Zeng, N., Karion, A., Mueller, K., Ghosh, S., Lopez-Coto, I., et al. (2019).  
 882 Investigating sources of variability and error in simulations of carbon dioxide in an urban  
 883 region. *Atmospheric Environment*, 199, 55–69.  
 884 <https://doi.org/10.1016/j.atmosenv.2018.11.013>
- 885 McDonald, B. C., McBride, Z. C., Martin, E. W., & Harley, R. A. (2014). High-resolution  
 886 mapping of motor vehicle carbon dioxide emissions. *Journal of Geophysical Research:*  
 887 *Atmospheres*, 119(9), 5283–5298. <https://doi.org/10.1002/2013JD021219>
- 888 McKain, K., Wofsy, S. C., Nehrkorn, T., Eluszkiewicz, J., Ehleringer, J. R., & Stephens, B. B.  
 889 (2012). Assessment of ground-based atmospheric observations for verification of  
 890 greenhouse gas emissions from an urban region. *Proceedings of the National Academy of*  
 891 *Sciences of the United States of America*, 109(22), 8423–8428.  
 892 <https://doi.org/10.1073/pnas.1116645109>
- 893 MDE (Maryland Department of the Environment). (2015). The Greenhouse Gas Emissions  
 894 Reduction Act Plan Update 2015. Retrieved March 17, 2019, from  
 895 <https://mde.maryland.gov/programs/marylander/documents/mccc/publications/2015ggraphlanupdate/climateupdate2015.pdf>
- 897 MDE (Maryland Department of the Environment). (2016). Maryland 2014 Periodic GHG  
 898 Emissions Inventory. Retrieved August 1, 2018, from  
 899 <https://mde.state.md.us/programs/Air/ClimateChange/Pages/GreenhouseGasInventory.aspx>
- 900 Mueller, K., Yadav, V., Lopez-Coto, I., Karion, A., Gourdji, S., Martin, C., & Whetstone, J.  
 901 (2018). Siting background towers to characterize incoming air for urban greenhouse gas  
 902 estimation: A case study in the Washington, DC/Baltimore area. *Journal of Geophysical*  
 903 *Research: Atmospheres*, 123(5), 2910–2926. <https://doi.org/10.1002/2017JD027364>
- 904 Nassar, R., Napier-Linton, L., Gurney, K. R., Andres, R. J., Oda, T., Vogel, F. R., & Deng, F.

- 905 (2013). Improving the temporal and spatial distribution of CO<sub>2</sub> emissions from global fossil  
906 fuel emission data sets. *Journal of Geophysical Research: Atmospheres*, *118*(2), 917–933.  
907 <https://doi.org/10.1029/2012JD018196>
- 908 Newman, S., Xu, X. M., Gurney, K. R., Hsu, Y. K., Li, K. F., Jiang, X., et al. (2016). Toward  
909 consistency between trends in bottom-up CO<sub>2</sub> emissions and top-down atmospheric  
910 measurements in the Los Angeles megacity. *Atmospheric Chemistry and Physics*, *16*(6),  
911 3843–3863. <https://doi.org/10.5194/acp-16-3843-2016>
- 912 O’Shea, S. J., Allen, G., Fleming, Z. L., Bauguitte, S. J. B., Percival, C. J., Gallagher, M. W., et  
913 al. (2014). Area fluxes of carbon dioxide, methane, and carbon monoxide derived from  
914 airborne measurements around Greater London: A case study during summer 2012. *Journal*  
915 *of Geophysical Research-Atmospheres*, *119*(8), 4940–4952.  
916 <https://doi.org/10.1002/2013JD021269>
- 917 Oda, T., & Maksyutov, S. (2011). A very high-resolution (1 km×1 km) global fossil fuel CO<sub>2</sub>  
918 emission inventory derived using a point source database and satellite observations of  
919 nighttime lights. *Atmos. Chem. Phys.*, *11*(2), 543–556. [https://doi.org/10.5194/acp-11-543-](https://doi.org/10.5194/acp-11-543-2011)  
920 [2011](https://doi.org/10.5194/acp-11-543-2011)
- 921 Oda, T., & Maksyutov, S. (2015). ODIAC fossil fuel CO<sub>2</sub> emissions dataset, Center for Global  
922 Environmental Research, National Institute for Environmental Studies.  
923 <https://doi.org/10.17595/20170411.001> (Access date: 2019/03/27).
- 924 Oda, T., Maksyutov, S., & Andres, R. J. (2018). The open-source data inventory for  
925 anthropogenic CO<sub>2</sub>, version 2016 (ODIAC2016): a global monthly fossil fuel CO<sub>2</sub> gridded  
926 emissions data product for tracer transport simulations and surface flux inversions. *Earth*  
927 *System Science Data*, *10*(1), 87–107. <https://doi.org/10.5194/essd-10-87-2018>
- 928 Oda, Tomohiro, Bun, R., Kinakh, V., Topylko, P., Halushchak, M., Marland, G., et al. (2019).  
929 Errors and uncertainties in a gridded carbon dioxide emissions inventory. *Mitigation and*  
930 *Adaptation Strategies for Global Change*, *24*(6), 1007–1050.  
931 <https://doi.org/10.1007/s11027-019-09877-2>
- 932 Patarasuk, R., Gurney, K. R., O’Keeffe, D., Song, Y., Huang, J., Rao, P., et al. (2016). Urban  
933 high-resolution fossil fuel CO<sub>2</sub> emissions quantification and exploration of emission drivers  
934 for potential policy applications. *Urban Ecosystems*, *19*(3), 1013–1039.  
935 <https://doi.org/10.1007/s11252-016-0553-1>
- 936 Peischl, J., Karion, A., Sweeney, C., Kort, E. A., Smith, M. L., Brandt, A. R., et al. (2016).  
937 Quantifying atmospheric methane emissions from oil and natural gas production in the  
938 Bakken shale region of North Dakota. *Journal of Geophysical Research-Atmospheres*,  
939 *121*(10), 6101–6111. <https://doi.org/10.1002/2015JD024631>
- 940 Peters, W., Jacobson, A. R., Sweeney, C., Andrews, A. E., Conway, T. J., Masarie, K., et al.  
941 (2007). An atmospheric perspective on North American carbon dioxide exchange:  
942 CarbonTracker. *Proceedings of the National Academy of Sciences*, *104*(48), 18925–18930.  
943 <https://doi.org/10.1073/pnas.0708986104>
- 944 Prairie, Y. T., & Duarte, C. M. (2007). Direct and indirect metabolic CO<sub>2</sub> release by humanity.  
945 *Biogeosciences*, *4*(2), 215–217. <https://doi.org/10.5194/bg-4-215-2007>
- 946 Quick, J. C., & Marland, E. (2019). Systematic error and uncertain carbon dioxide emissions  
947 from US power plants. *Journal of the Air & Waste Management Association*, 1–13.  
948 <https://doi.org/10.1080/10962247.2019.1578702>
- 949 Rayner, P. J., Raupach, M. R., Paget, M., Peylin, P., & Koffi, E. (2010). A new global gridded  
950 data set of CO<sub>2</sub> emissions from fossil fuel combustion: Methodology and evaluation.

- 951 *Journal of Geophysical Research-Atmospheres*, 115. <https://doi.org/10.1029/2009jd013439>
- 952 Ren, X., Salmon, O. E., Hansford, J. R., Ahn, D., Hall, D., Benish, S. E., et al. (2018). Methane  
953 emissions from the Baltimore-Washington area based on airborne observations:  
954 Comparison to emissions inventories. *Journal of Geophysical Research: Atmospheres*,  
955 123(16), 8869–8882. <https://doi.org/10.1029/2018JD028851>
- 956 Ren, X., Hall, D. L., Vinciguerra, T., Benish, S. E., Stratton, P. R., Ahn, D., et al. (2019).  
957 Methane emissions from the Marcellus shale in southwestern Pennsylvania and northern  
958 west Virginia based on airborne measurements. *Journal of Geophysical Research:*  
959 *Atmospheres*. <https://doi.org/10.1029/2018JD029690>
- 960 Salawitch, R. J., Canty, T. P., Hope, A. P., Tribett, W. R., & Bennett, B. F. (2017). *Paris climate*  
961 *agreement: Beacon of hope*. Springer International Publishing. [https://doi.org/10.1007/978-](https://doi.org/10.1007/978-3-319-46939-3)  
962 [3-319-46939-3](https://doi.org/10.1007/978-3-319-46939-3)
- 963 Salmon, O. E., Shepson, P. B., Ren, X., Collow, M., Allison, B., Miller, M. A., et al. (2017).  
964 Urban emissions of water vapor in winter. *Journal of Geophysical Research: Atmospheres*,  
965 122(17), 9467–9484. <https://doi.org/10.1002/2016JD026074>
- 966 Salmon, O. E., Shepson, P. B., Ren, X., He, H., Hall, D. L., Dickerson, R. R., et al. (2018). Top-  
967 down estimates of NO<sub>x</sub> and CO emissions from Washington, DC-Baltimore during the  
968 WINTER campaign. *Journal of Geophysical Research: Atmospheres*.  
969 <https://doi.org/10.1029/2018JD028539>
- 970 Sargent, M., Barrera, Y., Nehr Korn, T., Hutyr a, L. R., Gately, C. K., Jones, T., et al. (2018).  
971 Anthropogenic and biogenic CO<sub>2</sub> fluxes in the Boston urban region. *Proceedings of the*  
972 *National Academy of Sciences*, 115(29), 7491–7496.  
973 <https://doi.org/10.1073/pnas.1803715115>
- 974 Smith, I. A., Hutyr a, L. R., Reinmann, A. B., Thompson, J. R., & Allen, D. W. (2019). Evidence  
975 for edge enhancements of soil respiration in temperate forests. *Geophysical Research*  
976 *Letters*, 46(8), 4278–4287. <https://doi.org/10.1029/2019GL082459>
- 977 Stein, A. F., Draxler, R. R., Rolph, G. D., Stunder, B. J. B., Cohen, M. D., & Ngan, F. (2015).  
978 NOAA’s HYSPLIT atmospheric transport and dispersion modeling system. *Bulletin of the*  
979 *American Meteorological Society*, 96(12), 2059–2077. [https://doi.org/10.1175/BAMS-D-](https://doi.org/10.1175/BAMS-D-14-00110.1)  
980 [14-00110.1](https://doi.org/10.1175/BAMS-D-14-00110.1)
- 981 Stocker, T. F., D. Qin, Plattner, G.-K., Tignor, M., Allen, S. K., Boschung, J., et al. (2013). IPCC,  
982 2013: Climate Change 2013: The Physical Science Basis. Contribution of Working Group I  
983 to the Fifth Assessment Report of the Intergovernmental Panel on Climate Change.  
984 Retrieved November 28, 2018, from <https://www.ipcc.ch/report/ar5/wg1/>
- 985 Strong, C., Stwertka, C., Bowling, D. R., Stephens, B. B., & Ehleringer, J. R. (2011). Urban  
986 carbon dioxide cycles within the Salt Lake Valley: A multiple-box model validated by  
987 observations. *Journal of Geophysical Research: Atmospheres*, 116(D15).  
988 <https://doi.org/10.1029/2011JD015693>
- 989 Trainer, M., Ridley, B. A., Buhr, M. P., Kok, G., Walega, J., Hubler, G., et al. (1995). Regional  
990 ozone and urban plumes in the southeastern United-States - Birmingham, a case-study.  
991 *Journal of Geophysical Research-Atmospheres*, 100(D9), 18823–18834.  
992 <https://doi.org/10.1029/95JD01641>
- 993 Turnbull, J., Sweeney, C., Karion, A., Newberger, T., Lehman, S. J., Tans, P. P., et al. (2015).  
994 Toward quantification and source sector identification of fossil fuel CO<sub>2</sub> emissions from an  
995 urban area: Results from the INFLUX experiment. *Journal of Geophysical Research:*  
996 *Atmospheres*, 120(1), 292–312. <https://doi.org/10.1002/2014JD022555>

- 997 Turnbull, J., Karion, A., Davis, K. J., Lauvaux, T., Miles, N. L., Richardson, S. J., et al. (2018).  
998 Synthesis of urban CO<sub>2</sub> emission estimates from multiple methods from the Indianapolis  
999 Flux Project (INFLUX). *Environmental Science & Technology*, 53(1), 287–295.  
1000 <https://doi.org/10.1021/acs.est.8b05552>
- 1001 UN-Habitat (United Nations Human Settlements Programme). (2011). *Cities and climate change:  
1002 Global report on human settlements 2011* (illustrate). Earthscan. Retrieved from  
1003 <https://books.google.com/books?id=dzJhJny37h8C>
- 1004 UN (United Nations). (2017). Reference: C.N.464.2017.TREATIES-XXVII.7.d (Depositary  
1005 Notification). Retrieved May 10, 2019, from  
1006 <https://treaties.un.org/doc/Publication/CN/2017/CN.464.2017-Eng.pdf>
- 1007 USEIA (US Energy Information Administration). (2016). Layer Information for Interactive State  
1008 Maps: Power Plants. Retrieved March 1, 2016, from [https://www.eia.gov/maps/layer\\_info-  
1010 m.php](https://www.eia.gov/maps/layer_info-<br/>1009 m.php)
- 1010 USEPA (U.S. Environmental Protection Agency). (2009). Plain English Guide to the Part 75  
1011 Rule. Retrieved May 10, 2019, from [https://www.epa.gov/sites/production/files/2015-  
1012 05/documents/plain\\_english\\_guide\\_to\\_the\\_part\\_75\\_rule.pdf](https://www.epa.gov/sites/production/files/2015-<br/>1012 05/documents/plain_english_guide_to_the_part_75_rule.pdf)
- 1013 USEPA AMPD (U.S. Environmental Protection Agency). (2015). Air Markets Program Data  
1014 (AMPD). Retrieved August 1, 2015, from <https://ampd.epa.gov/ampd/>
- 1015 USEPA GHGRP (U.S. Environmental Protection Agency). (2019). Greenhouse Gas Reporting  
1016 Program (GHGRP). Retrieved March 1, 2017, from <https://www.epa.gov/ghgreporting>
- 1017 Whetstone, J. R. (2018). Advances in urban greenhouse gas flux quantification: The Indianapolis  
1018 Flux Experiment (INFLUX). *Elem Sci Anth*, 6(1). <https://doi.org/10.1525/elementa.282>
- 1019 White, W. H., Patterson, D. E., & Wilson, W. E. (1983). Urban exports to the nonurban  
1020 troposphere: Results from Project MISTT. *Journal of Geophysical Research: Oceans*.  
1021 <https://doi.org/10.1029/JC088iC15p10745>
- 1022 Zeng, N., Qian, H., Munoz, E., & Iacono, R. (2004). How strong is carbon cycle-climate  
1023 feedback under global warming? *Geophysical Research Letters*, 31(20).  
1024 <https://doi.org/10.1029/2004GL020904>
- 1025 Zeng, N., Mariotti, A., & Wetzol, P. (2005). Terrestrial mechanisms of interannual CO<sub>2</sub>  
1026 variability. *Global Biogeochemical Cycles*, 19(1). <https://doi.org/10.1029/2004GB002273>  
1027  
1028

1029 **Table 1.** Summary of the mass balance parameters used to estimate the emissions of CO<sub>2</sub> from  
 1030 the Balt-Wash area. For the boundary layer height ( $z_f$ ), the best estimates and  $1\sigma$  uncertainties are  
 1031 shown. For the mole fraction of CO<sub>2</sub> ( $[\text{CO}_2]$ ), CO<sub>2</sub> background ( $[\text{CO}_{2,bg}]$ ), perpendicular wind  
 1032 speed ( $U$ ), and the wind variability during air transport across the study area ( $k$ ), the mean and  
 1033 the standard deviation during the downwind flight period are shown (See section 2.5). The flux  
 1034 of CO<sub>2</sub> was calculated for each point in each transect, and thus the mean  $[\text{CO}_2]$ ,  $[\text{CO}_{2,bg}]$ ,  $U$ , and  
 1035  $k$  values thus not directly translate into the mass balance estimate results.

	Date	$z_f \pm 1\sigma$ [m]	$[\text{CO}_2] \pm 1\sigma$ [ppm]	$[\text{CO}_{2,bg}] \pm 1\sigma$ [ppm]	$\bar{U} \pm 1\sigma$ [m/s]	$\bar{k} \pm 1\sigma$
UMD-RF4	Feb 19 2015	1,372 ± 280	409.3 ± 0.8	408.5 ± 0.3	12.8 ± 1.6	0.95 ± 0.01
UMD-RF5	Feb 20 2015	1,109 ± 139	411.2 ± 1.4	409.4 ± 0.2	5.6 ± 1.4	0.75 ± 0.04
UMD-RF6	Feb 23 2015	1,013 ± 265	406.8 ± 1.1	405.7 ± 0.4	10.6 ± 1.5	1.06 ± 0.01
UMD-RF8	Feb 25 2015	1,393 ± 137	410.1 ± 1.9	408.6 ± 0.9	5.3 ± 2.0	0.91 ± 0.05
UMD-RF9	Feb 26 2015	896 ± 268	417.9 ± 2.5	414.2 ± 0.8	3.9 ± 1.1	0.90 ± 0.04
Purdue-RF3	Feb 19 2015	1,372 ± 280	410.0 ± 0.5	409.2 ± 0.2	12.7 ± 1.3	1.00 ± 0.02
Purdue-RF4	Feb 27 2015	1,626 ± 349	414.3 ± 2.4	412.6 ± 0.6	5.1 ± 1.6	0.98 ± 0.04

1036

1037 **Table 2.** Sensitivity test for the aircraft-based mass balance estimates of the emission of CO<sub>2</sub>  
 1038 from the Balt-Wash area. Baseline estimates from the seven flights are shown on the first row.  
 1039 Relative differences indicate the changes of the baseline estimate when the  $\pm 1\sigma$  uncertainty of  
 1040 each mass balance parameter is used to calculate the emission of CO<sub>2</sub>. The total  $1\sigma$  uncertainty  
 1041 of each baseline estimate is shown as the relative standard deviation (RSD) at the bottom row.  
 1042 On the column labeled “Mean”, the mean and SEM95 values of seven Baseline estimates were  
 1043 shown in the first row, and the mean values were shown for the remaining rows.  
 1044

	UMD					Purdue		Mean
	RF4	RF5	RF6	RF8	RF9	RF3	RF4	
	Feb 19	Feb 20	Feb 23	Feb 25	Feb 26	Feb 19	Feb 27	
<b>Baseline estimates [<math>10^5</math> mol/s]</b>	1.10	0.68	0.98	0.79	0.74	1.09	0.89	0.89 ± 0.15
<b>Relative Differences (RD) [%]</b>								
Wind variability, Downwind	± 13	± 25	± 14	± 39	± 29	± 18	± 39	± 25
PBL height	± 20	± 13	± 27	± 10	± 30	± 20	± 21	± 20
CO <sub>2</sub> background	± 19	± 11	± 16	± 9	± 19	± 18	± 20	± 16
Instruments (Temp, Pres, CO <sub>2</sub> )	± 8	± 3	± 6	± 4	± 2	± 11	± 5	± 5
Wind variability, Transport	± 1	± 4	± 1	± 4	± 6	± 2	± 3	± 3
<b>Total uncertainty [RSD, %]</b>	± 32	± 31	± 34	± 41	± 49	± 33	± 49	± 38

1045

1046 **Figure 1.** Overview of the FLAGG-MD aircraft campaign during February 2015 conducted in  
1047 the Baltimore, MD and Washington, D.C. metropolitan areas; the white rectangle defines the  
1048 Balt-Wash study area used throughout the analysis. Yellow and cyan lines indicate the UMD and  
1049 Purdue aircraft flight tracks, respectively. The dominant wind direction during the campaign  
1050 period is shown by the white arrow. Point emission sources are shown as circles; the size and  
1051 color of these circles indicate the amount of CO<sub>2</sub> (size) and SO<sub>2</sub> (color) emitted from these  
1052 sources in February 2015 (USEPA AMPD 2015). The VP labels indicate locations where vertical  
1053 profile data were obtained. The points labeled A, B, C, and D denote the edge of the region for  
1054 which the emission of CO<sub>2</sub> from the Balt-Wash region is found. The boundary of the vertical  
1055 plane AB, for which transects at various altitudes were flown, is used to define the downwind  
1056 study area to calculate the emission of CO<sub>2</sub> for all flights except UMD-RF9. The vertical plane  
1057 BC is used to define the downwind boundary for UMD-RF9, since northeasterly winds were  
1058 present on 26 February 2015.  
1059

1060 **Figure 2.** Scatter plot of the upwind CO<sub>2</sub> mole fraction (10 second running mean) versus the  
1061 paired downwind, background estimate of CO<sub>2</sub>. The number of paired data points for each flight  
1062 is indicated on panel (a); the total number of paired points (5882) yields a mean and standard  
1063 deviation of  $0.18 \pm 0.79$  ppm. Panel (b) shows the mixed layer depth extracted from HYSPLIT  
1064 run using North American Regional Reanalysis (NARR) meteorological fields along the upwind  
1065 aircraft flight track and the location of the paired, downwind data. Results are shown for six of  
1066 the seven mass balance flights considered in the analysis, because upwind measurements of CO<sub>2</sub>  
1067 were not obtained for UMD-RF9.  
1068

1069 **Figure 3.** (a) Colored lines depict back trajectories initiated along the aircraft track, downwind of  
1070 the Balt-Wash area on 20 February 2015 (UMD-RF5). Triangles indicate the locations of back  
1071 trajectories at every hour. Black circles indicate the major power plants in the study area. Mean  
1072 aircraft altitude and the wind speed and direction measured during the flight are shown in the left  
1073 box. (b) Time series of mole fractions of CO<sub>2</sub> and SO<sub>2</sub> measured during the same flight track.  
1074 Green shaded areas indicate the plumes partially attributed to local power plants while the grey  
1075 shaded areas indicate urban plumes. The DC+ $\alpha$  label indicates that the plume is attributed to  
1076 Washington, D.C. and nearby Dickerson power plant. The Balt+ $\beta$  label indicates that the plume  
1077 is attributed to Baltimore, MD and to major power plants in Pennsylvania (labelled as PA in the  
1078 map, see Figure 4 for further analysis). See section 3.5.1 for detailed spatial distribution of fossil-  
1079 fuel CO<sub>2</sub> flux over the study area.  
1080

1081 **Figure 4.** (a-f) Colored circles show mole fractions of SO<sub>2</sub> measured during six flights in  
1082 February 2015. Colored lines are back trajectories initiated at the location of the SO<sub>2</sub> plume  
1083 observed downwind of the Balt-Wash area. Triangles on each trajectory show the location at  
1084 every hour. Mean wind measured during the downwind flight is shown at the left-bottom corner  
1085 of each panel. (g) A map showing same flight tracks and trajectories of (a-f) in a larger domain.  
1086 The dashed box encloses the locations of five major power plants in Pennsylvania. The names of  
1087 power plants, fuel, and their nameplate capacity are shown at the left-bottom corner (Source:  
1088 USEIA, 2016).  
1089

1090 **Figure 5.** Maps showing HYSPLIT particle dispersion simulations of power plant emissions of  
 1091 CO<sub>2</sub> and flight tracks of (a) UMD-RF4 and (b) UMD-RF5. “HYSPLIT CO<sub>2</sub>” labels (color bars  
 1092 and Y axes) indicate the enhancement of CO<sub>2</sub> due to power plant emissions averaged within the  
 1093 boundary layer. “Aircraft CO<sub>2</sub>” labels indicate measured mole fractions of CO<sub>2</sub> for a single  
 1094 transect, along the line A at 707 m (UMD-RF4) and 614 m (UMD-RF5) altitude. The location of  
 1095 power plant point emission sources used for the modeling are shown as pink circles. (c, d) Time  
 1096 series of “Aircraft CO<sub>2</sub>” at 707 m (UMD-RF4) and 614 m (UMD-RF5) altitude along the line  
 1097 AB and stacked bar plots of “HYSPLIT CO<sub>2</sub>” that were sampled for aircraft locations of the in-  
 1098 situ data. Each color of the bar indicates the state or region where the sampled HYSPLIT CO<sub>2</sub>  
 1099 was emitted; i.e., emissions from the study area are denoted as DC/Balt. The percentage of  
 1100 power plant emissions from region, for the given transects, is also provided (numbers sum to  
 1101 100%).  
 1102

1103 **Figure 6.** (a) Emission of CO<sub>2</sub> from the Chalk Point and Morgantown power plants in units of  
 1104 metric tons of carbon per hour. Black lines indicate the reported CEMS emission rates. Red and  
 1105 green diamonds represent the emission rates that we estimated using in-situ measurements from  
 1106 the UMD and Purdue aircraft, respectively. (b) Scatter plot showing the comparison of the same  
 1107 dataset in (a). Dotted and solid lines indicate 1 to 1 ratio and linear regression lines, respectively.  
 1108 Vertical error bars on each diamond indicate the 1 $\sigma$  uncertainty induced by the uncertainty in the  
 1109 adjusted mixing height ( $z_{adj}$ ) (section 2.5.3). Horizontal error bars indicate the combined  
 1110 uncertainty of the CEMS records and the plume transport time (See Text S4).  
 1111

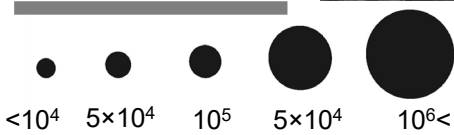
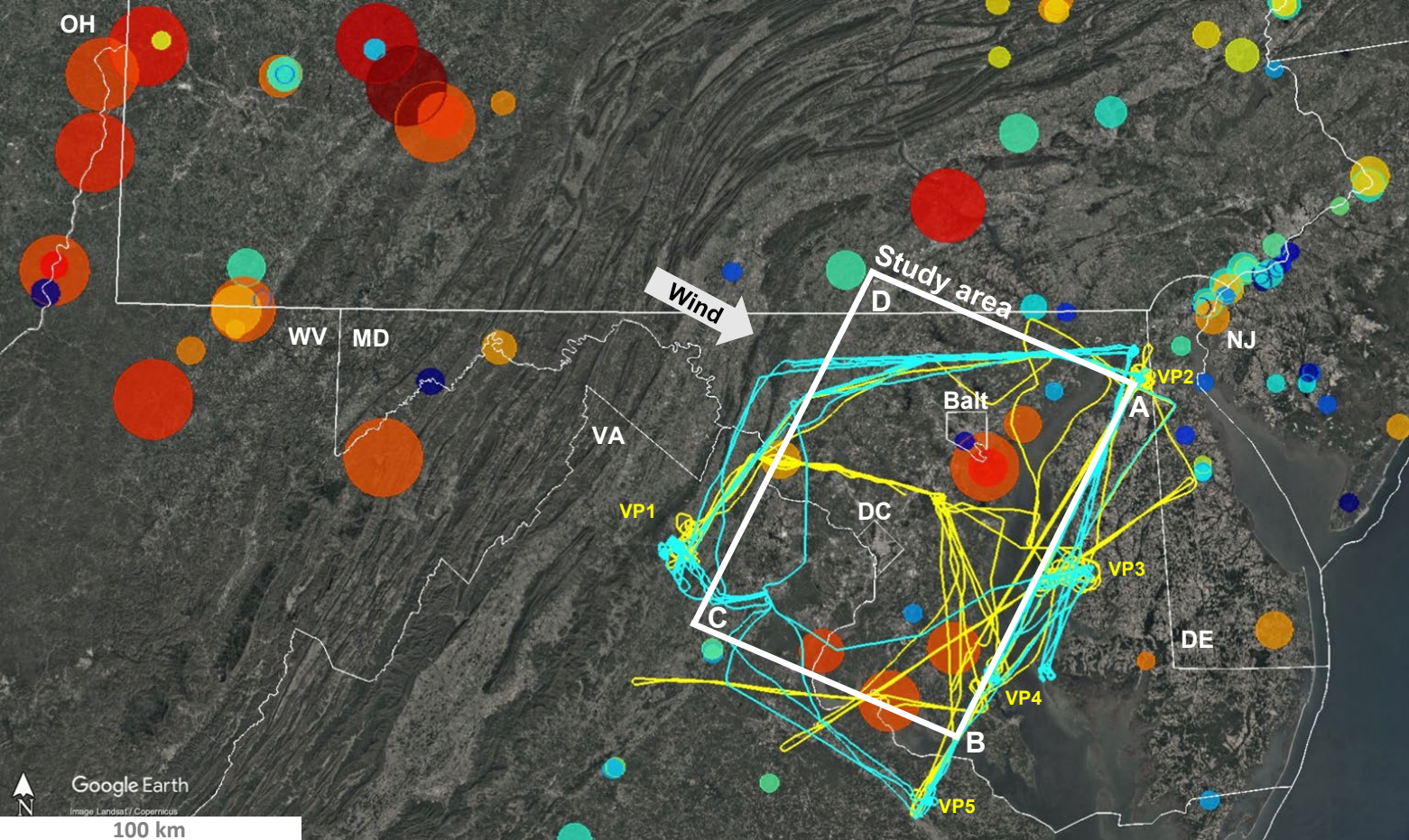
1112 **Figure 7.** Maps of FFCO<sub>2</sub> flux over the Mid-Atlantic region from (a) ACESv1, (b) ODIAC2018,  
 1113 (c) FFDASv2.2, (d) EDGARv432, (e) CT2017. The Balt-Wash study area is indicated as a red  
 1114 box. (f) Horizontal transects of CO<sub>2</sub> flux derived from the biogenic model (VEGAS+NDVI) and  
 1115 the five FFCO<sub>2</sub> products (Unit: Million tons Carbon (MtC) per month). These transects were  
 1116 obtained by summing the flux along diagonal latitudinal bins, as indicated by four grey shaded  
 1117 areas shown in panel (e) and (f) (SE corner and NE corner of a red box, Washington, D.C. and  
 1118 Baltimore). The x-axis in (f) represents the latitudes along the line AB shown in panel (e). For  
 1119 major spikes, abbreviated names of the power plants are shown (see Figure 3).  
 1120

1121 **Figure 8.** The emission rates of CO<sub>2</sub> from the Balt-Wash area during the sampling period of  
 1122 seven research flights in February 2015. Solid bars and their black vertical lines indicate the  
 1123 seven FLAGG-MD baseline estimates and their 1 $\sigma$  uncertainty range (Table 2). FLAGG-MD  
 1124 mass balance estimates were apportioned to FFCO<sub>2</sub> (purple), Non-FFCO<sub>2</sub> Anthropogenic  
 1125 emissions (NFA-CO<sub>2</sub>, blue) and the human/pet respiration (yellow) (See Text S5). Dashed bars  
 1126 indicate corresponding FFCO<sub>2</sub> from FFDASv2.2. The black vertical lines at the top of the  
 1127 FFDASv2.2 bars (dashed) indicate the minimum to maximum hourly emission rates of FFCO<sub>2</sub>  
 1128 for each time period, and thus are not an uncertainty estimate of FFDASv2.2.  
 1129  
 1130

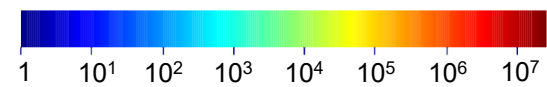
1131 **Figure 9.** Monthly emission of CO<sub>2</sub> from the Balt-Wash area for February 2015. The emission  
 1132 by human/pet respiration (yellow) was estimated using population data (GPWv4, (CIESIN,  
 1133 2018)) and the average respiration rate from Prairie & Duarte (2007) (see Text S5). Non-FFCO<sub>2</sub>  
 1134 Anthropogenic emissions (NFA-CO<sub>2</sub>, blue) were calculated from FLAGG-MD mass balance  
 1135 estimates using the scaling factor derived from the MDE GHG inventory 2014 (MDE, 2016).

1136 EDGARv432 and ACESv1 were available for 2010 and 2014, respectively. The four bottom-up  
1137 FFCO<sub>2</sub> estimates (ODIAC2018, EDGARv432, ACESv1, and FFDASv2.2) contain several  
1138 mismatching emission sectors, and thus are not directly comparable (see text). Sectoral emissions  
1139 from EDGARv432 and ACESv1 were aggregated into four categories: electricity generating  
1140 facilities (“ELEC”, diagonal), residential, commercial, and industrial (“RCI”, dotted), on-road  
1141 (horizontal) and non-road transportation (vertical). See Text S6 for emission sectors covered by  
1142 each bottom-up product. The “Bottom-Up Mean” bar and its vertical error bar indicate the mean  
1143 and standard deviation of the four bottom-up FFCO<sub>2</sub> estimates. The error bar on the FLAGG-  
1144 MD symbol indicates the  $1\sigma$  uncertainty range of the best estimate.  
1145

Figure 1 (pdf).



CO<sub>2</sub> (Short tons)



SO<sub>2</sub> (Pounds)

Figure 2.

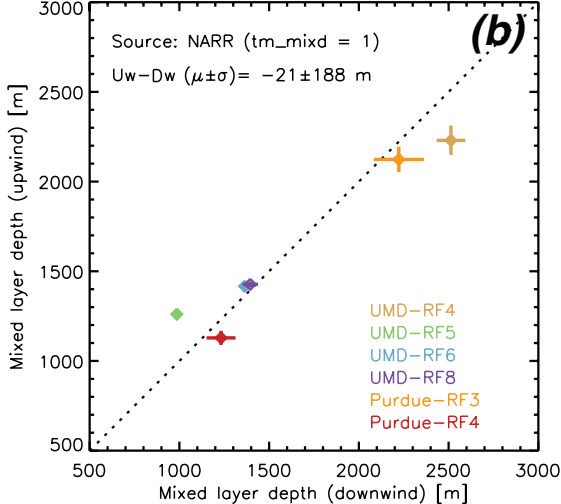
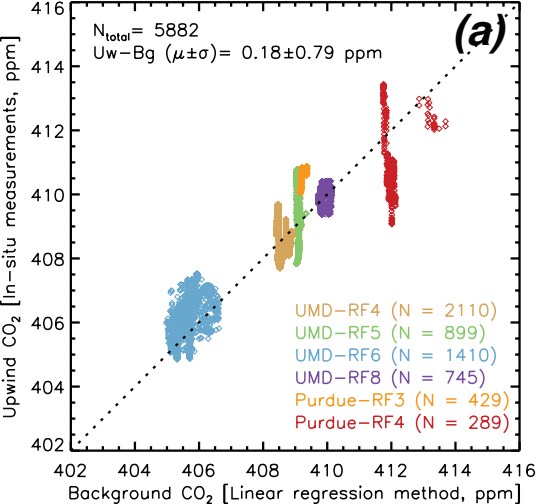
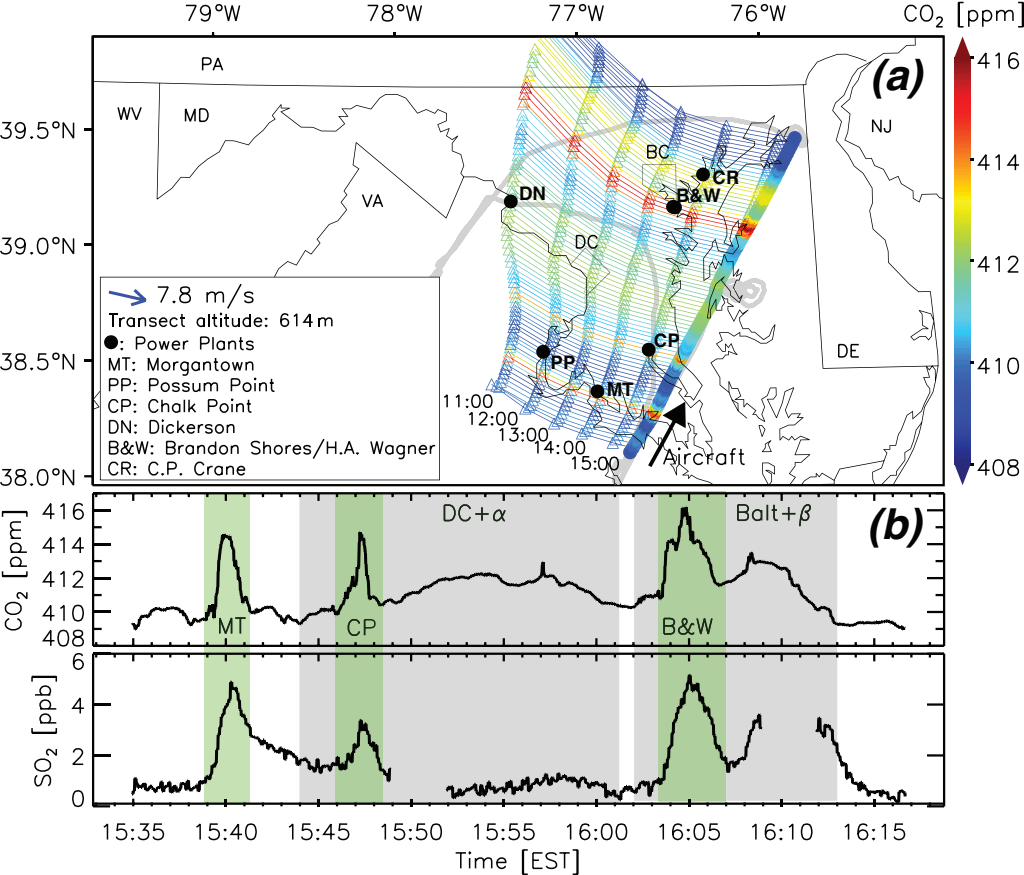


Figure 3.



**Figure 4.**

HYSPLIT: Start off from downwind of Balt-Wash area

Aircraft: 30s avg. SO<sub>2</sub>, (5th–95th percentile)

SO<sub>2</sub> [ppb]

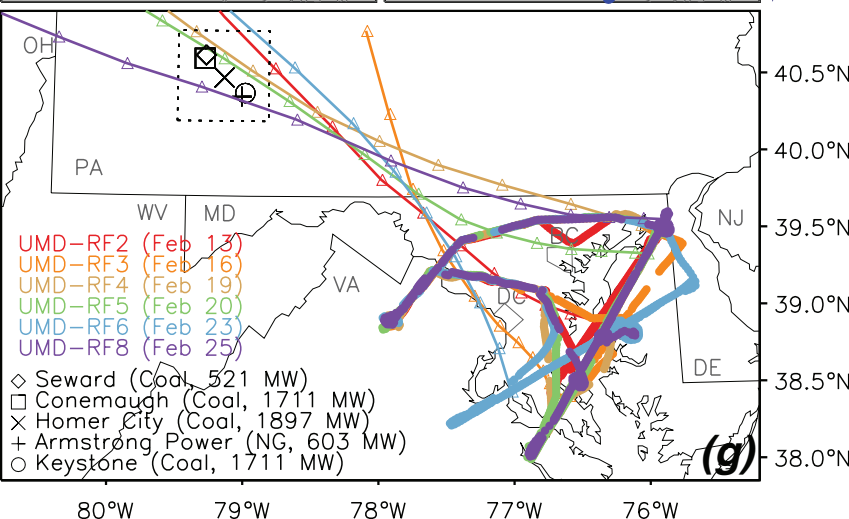
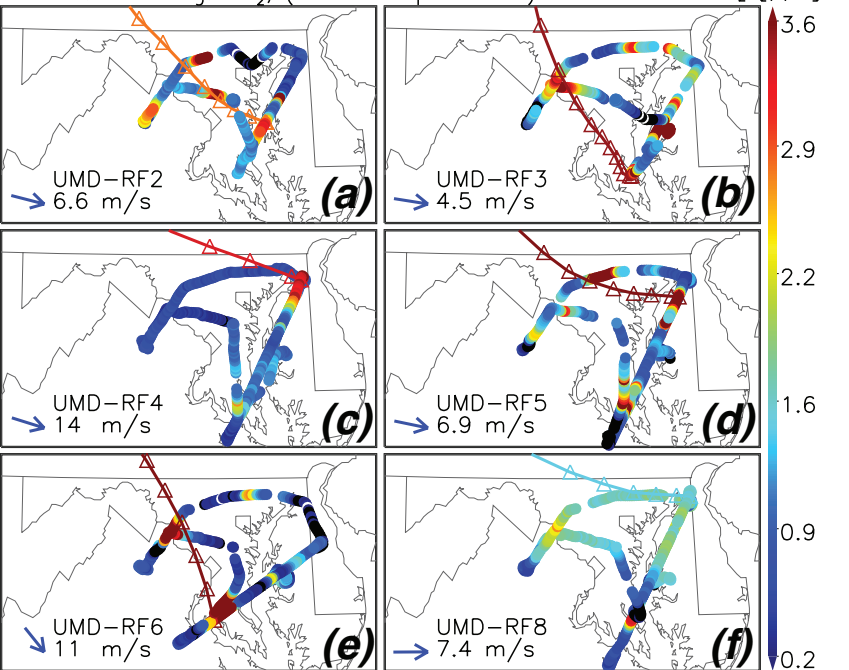
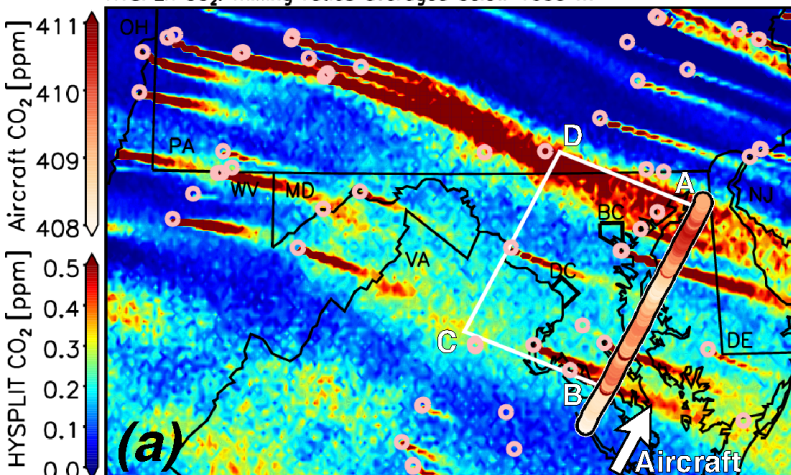


Figure 5.

Snapshot at 15:47 Feb 19 2015  
 Aircraft CO<sub>2</sub>: In-situ measurements at 707 m (UMD-RF4)  
 HYSPLIT CO<sub>2</sub>: mixing ratios averaged below 1000 m



Snapshot at 16:33 Feb 20 2015  
 Aircraft CO<sub>2</sub>: In-situ measurements at 614 m (UMD-RF5)  
 HYSPLIT CO<sub>2</sub>: mixing ratios averaged below 1000 m

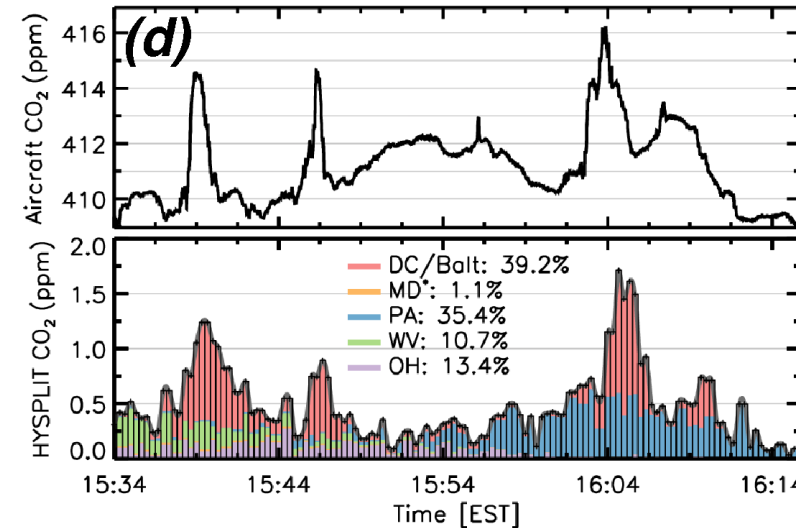
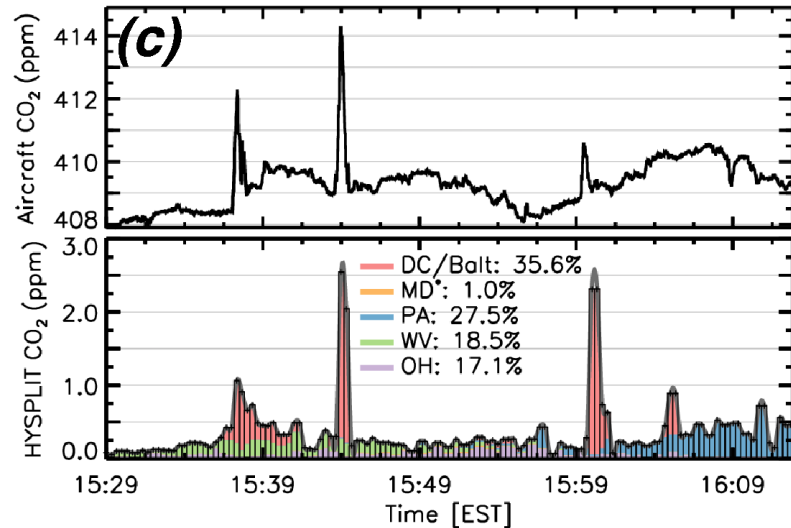
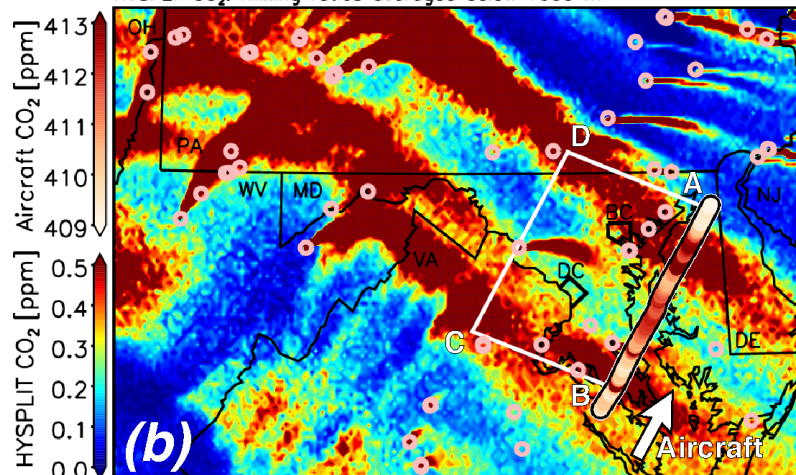
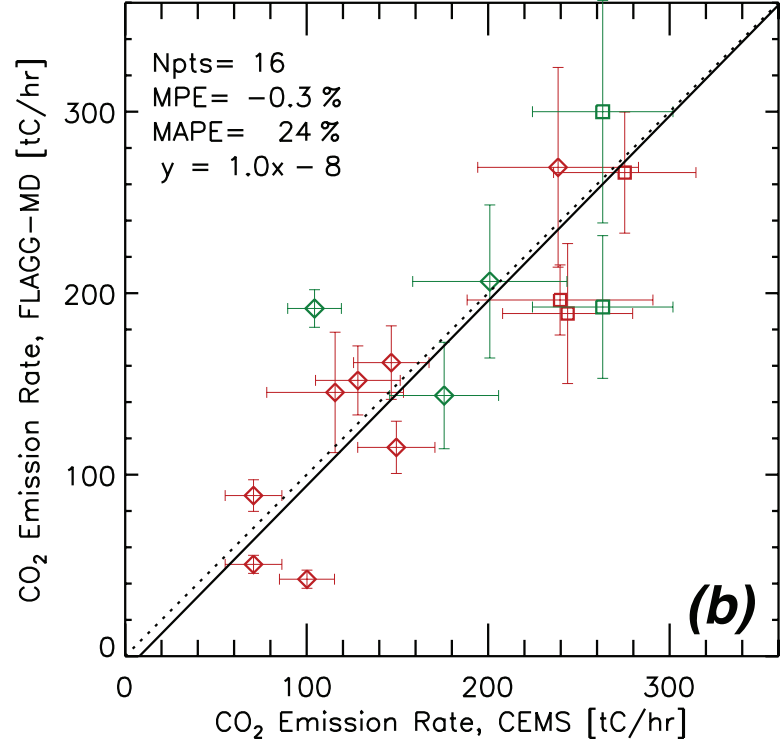
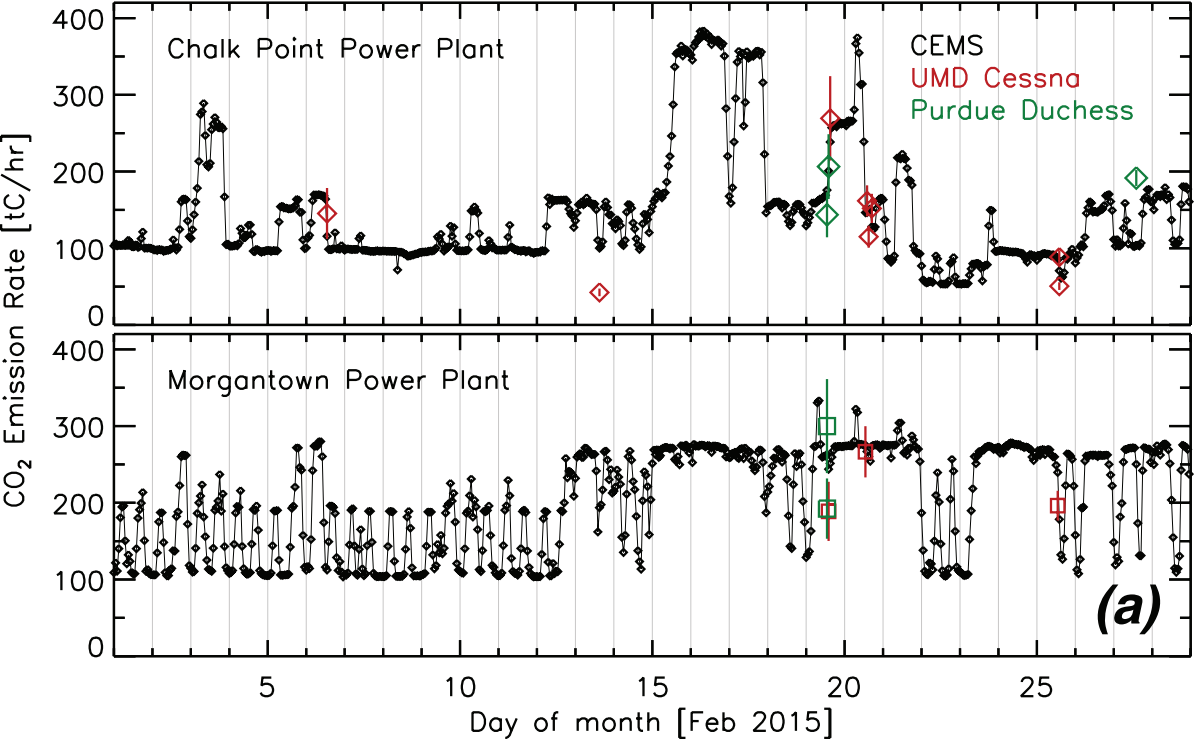
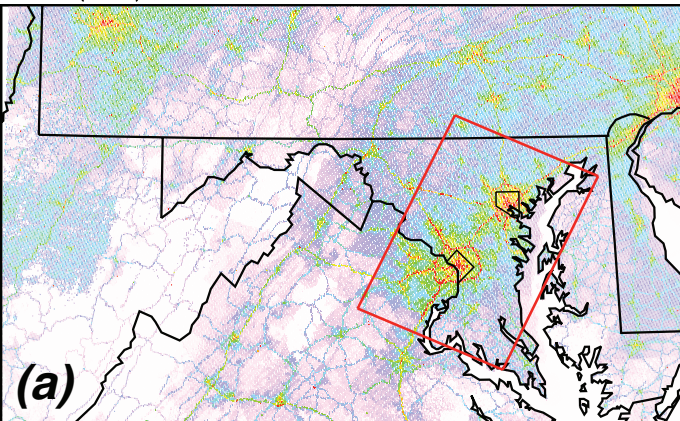


Figure 6.

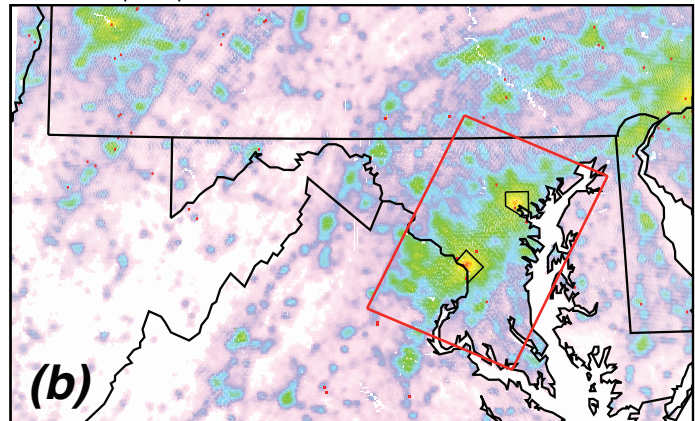


**Figure 7.**

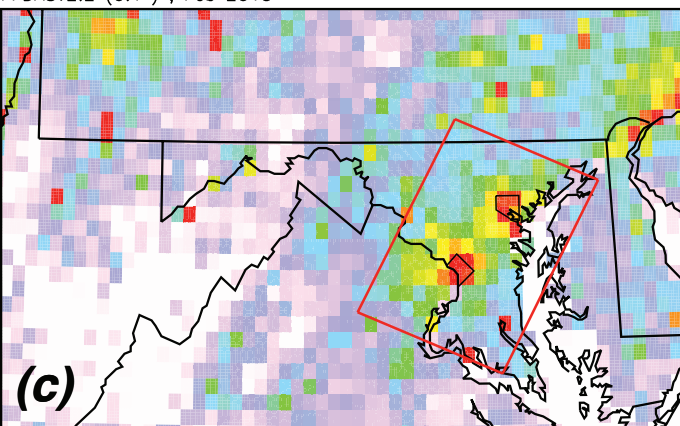
ACESv1 (1 km), Feb 2014



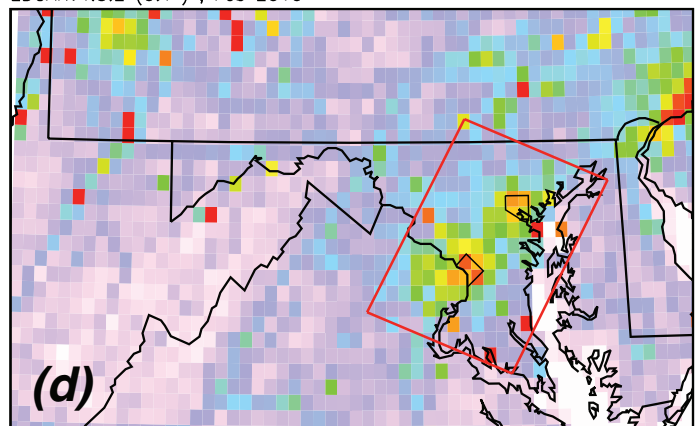
ODIAC2018 (1 km), Feb 2015



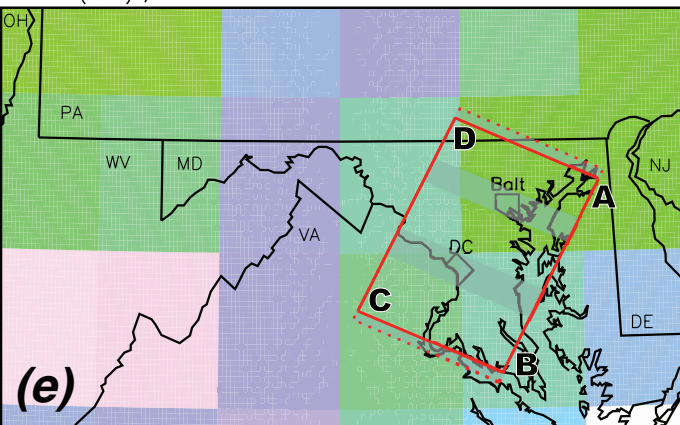
FFDASv2.2 (0.1°), Feb 2015



EDGARv4.3.2 (0.1°), Feb 2010



CT2017 (1.0°), Feb 2015



Emissions of CO<sub>2</sub> [MtC/month]

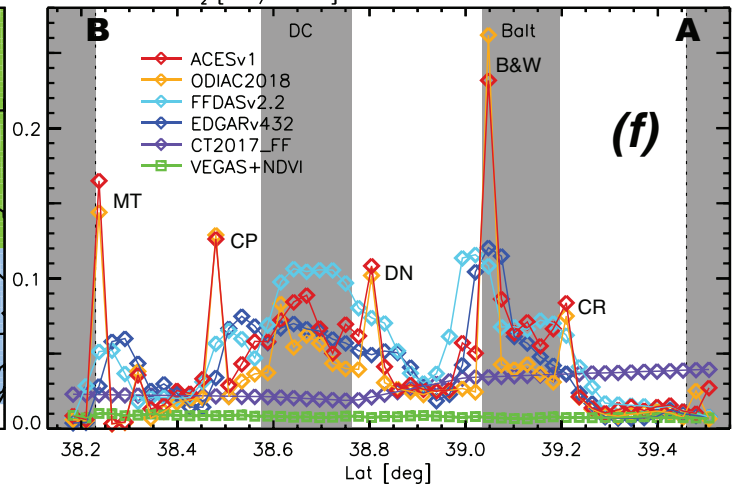


Figure 8.

Balt-Wash area, Feb 2015

Emission rate of CO<sub>2</sub> [10<sup>5</sup> moles/s]

Fossil fuel combustion (Solid:FLAGG-MD, Dashed:FFDASv2.2)  
 Biotic fuel, Industrial processes, Agriculture, Waste management  
 Human & pet respiration

MPE = 32 %

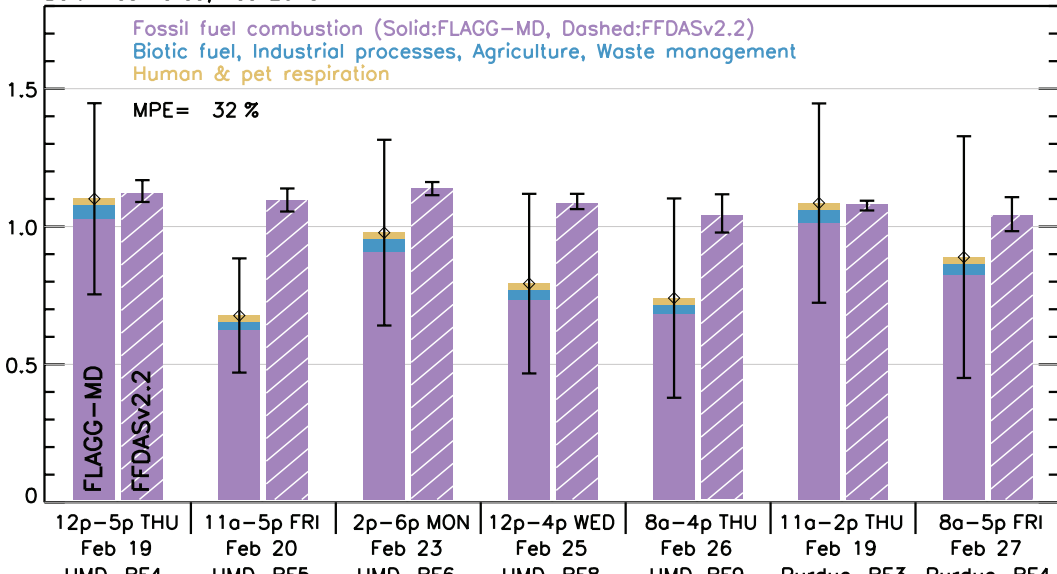


Figure 9.

